# ON-MACHINE PROBING TO IDENTIFY GEOMETRIC VARIATIONS OF FORGINGS

By

ARTHUR ANDRADE GRAZIANO

A THESIS PRESENTED TO THE GRADUATE SCHOOL
OF THE UNIVERSITY OF FLORIDA IN PARTIAL FULFILLMENT
OF THE REQUIREMENTS FOR THE DEGREE OF
MASTER OF SCIENCE

UNIVERSITY OF FLORIDA

2010

To my family

ACKNOWLEDGMENTS

I thank my adviser Dr. Tony Schmitz, Dr. Dean Bartles, General Dynamics-OTC, for financial support, and my coworkers at the Machine Tool Research Center (MTRC).

TABLE OF CONTENTS

APPENDIX

LIST OF TABLES

LIST OF FIGURES

## LIST OF ABBREVIATIONS

| | |
|---|---|
| CMM | Coordinate Measuring Machine |
| CNC | Computer Numerical Controlled |
| LVDT | Linear Variable Differential Transformer |

Abstract of Thesis Presented to the Graduate School
of the University of Florida in Partial Fulfillment of the
Requirements for the Degree of Master of Science

ON-MACHINE PROBING TO IDENTIFY GEOMETRIC VARIATIONS OF FORGINGS

By

Arthur Andrade Graziano

May 2010

Chair: Tony L. Schmitz
Major: Mechanical Engineering

Tool joints are manufactured by General Dynamics at their production facility in Red Lion, Pennsylvania. The joints are initially forged (from raw stock) and then machined to final dimensions. One obstacle to optimized turning performance is that the forgings include deviations from the nominal dimensions, including length variations and non-concentricity of the inner and outer diameters. This causes more or less material to be removed than anticipated during turning, boring, and facing operations and requires that a conservative machining approach be applied to avoid larger depths of cut than planned and the subsequent tool/workpiece damage and/or accelerated tool wear. Although on-machine probing may be used to verify final workpiece dimensions (after machining), it is not typically used to measure coarse workpiece dimensions prior to machining due to the rough and inconsistent nature of the workpiece.

In order to provide pre-machining measurements of forging dimensions, two linear variable differential transformer (LVDT) contact probes were developed to measure the length and concentricity of the cylindrical tool joint workpieces when clamped in a computer numerical controlled (CNC) lathe. The probes consisted of a LVDT, linear shaft, and hardened steel spheres to contact the rough workpiece. For concentricity

measurements, a parallelogram leaf-type flexure and 45° platform was used to transfer motion to the LVDT axis. The CNC machine scales were used in conjunction with the sensor output to determine the forged part dimensions.

The devices were used to measure 12 forged workpieces provided by General Dynamics. Both probes showed acceptable measurement repeatability. When measuring the same workpiece, the average range in values for length, radius, and center offset were 8 µm, 3 µm, and 1 µm respectively, which correspond to 0.001%, 0.006%, and 0.59% change variation, respectively. While the mean value for length was within the forging design tolerance, the radius measurements were smaller than the provided tolerance. It is believed that this bias was caused by rust and other debris on the inside of the forged workpieces being dragged by the contact sphere and forming a thin layer between the contact sphere and workpiece surface.

In addition, an artifact with known dimensions was measured to verify the devices' accuracy. The devices were accurate to within 0.007% and 0.053% when measuring length and radius, respectively. Center offset was difficult to measure accurately due to the lack of an encoder to synchronize the rotation of the spindle to the acquired data.

# CHAPTER 1
# INTRODUCTION

Tool joints are an essential component in the oil drilling industry. They provide a strong connection between individual drill pipes that must withstand extraordinary pressures. General Dynamics produces such parts at their Ordnance and Tactical Systems facility in Red Lion, Pennsylvania. Figure 1-1 shows a pallet of tool joints manufactured at Red Lion.

The manufacturing process for these parts requires several steps. First, raw stock arrives in long, solid, steel cylinders and is sheared to length using a 400 T press at 2100 ºF. Next, the parts go through a pin-and-box reverse extrusion process to produce the basic shape depicted in Figure 1-2. A schematic of the process is shown in Figure 1-3 [1].

These forged parts are allowed to cool outside before being transferred to the shop floor for the final machining process [1]. During this cooling process, a significant amount of rust develops on the surface of the workpieces; this becomes a factor later in the manufacturing process. The forged part weighs approximately 76 kg and its dimensions in inches are shown in Figure 1-4. At the shop floor, two separate machining operations are performed in order to achieve the final desired geometry shown in Figure 1-5.

The forged parts are machined on Okuma LC-40 lathes. See Figure 1-6. The lathe consists of two independent turrets. Turret A (top turret) performs boring and drilling operations, while turret B (bottom turret) performs facing and turning cuts. The turrets are capable of moving in two directions. The Z axis is defined as the axis of symmetry of the spindle. The Z axis is measured in inches and is displayed with a resolution of ten

thousandths of an inch on the lathe controller interface. The X axis is the diametral axis and it moves out from the center of the spindle at an angle of 60° from horizontal. The same units are displayed for this axis; however, it corresponds to a diameter, such that for every inch that the turret is displaced, the axis value increases by two inches (diameter value). The lathe weighs approximately 10500 kg and has a maximum turning diameter of 400 mm and a maximum working length of 750 mm. The main spindle is rated to maintain 37 kW of continuous power.

Many problems arise during machining due to the forging process. These can be attributed to three process inconsistencies.

1. Since the material is allowed to flow up and around the pin when extruded, a bulge can be created and the end is not flat. The peak of the bulge is located somewhere between the inner and outer diameter, but not necessarily at the middle.
2. The precise temperature of the workpiece once it reaches the extrusion process is unknown, so the amount of thermal deformation cannot be accurately predicted. Length variations are therefore inherent to the forging process and account for one of the main problems during machining: unknown part length.
3. The final inconsistency in the forging process accounts for the following two problems encountered during machining. After many cycles of extrusion, the pin may lose its perpendicularity to the part axis and no longer begins its extrusion at the workpiece center. This creates a part with a hole that is off-center from the center axis. In addition, as the extrusion proceeds, the pin may be deflected to one side, causing a non-concentric hole with respect to the outside surface. See Figure 1-7. Since workpieces are chucked on the outside during the machining process, this latter problem reveals itself as runout when turning the inside diameter. The outside diameter is assumed consistent (based on shop floor experience) and is not considered here.

The current solution being implemented to solve these problems requires measuring the forged parts every hour and stopping production for maintenance on the pin once a part is tested that is out of tolerance. Although the pin can be reset, there is no correction in place for the length variation. Since many parts still get passed before a problem is noticed, an extremely conservative machining pass is necessary in both the

facing operation and the boring operation in order to prevent tool/part damage and/or potential machine failure from an excessive depth of cut. Tool wear is also naturally a consideration, but cannot be prevented due to the nature of the cutting process.

In this work an alternate solution to the conservative and time-consuming machining strategy is proposed. Rather than using a part program adapted to the worst case dimensional variation, the workpieces dimensions can be determined by contact probing on the machine (prior to performing the cutting operations). If the part dimensions can be accurately and quickly identified using the in-process probing strategy, then the part program can be modified in real time, or an appropriate program can be selected from a matrix of programs based on the measured dimensions. The new program would account for any dimensional inaccuracies generated during the forging process. The goal of this solution is to eliminate redundant operations and reduce machining time, thereby reducing the cost per part. If the probes are mounted on the turret similar to a tool, workpiece measurements can be completed in order to obtain its actual dimensions. The probes must satisfy certain requirements, however, in order to be useful for this task. They must be sufficiently accurate and robust enough to survive in the machining environment. The diametral probe must be small enough to fit inside and long enough to measure deep within the workpieces. Additionally, the probes must perform measurements quickly in order to be cost effective for the given process.

Figure 1-1. Machined tool joints [1].

Figure 1-2. Typical forged workpiece.

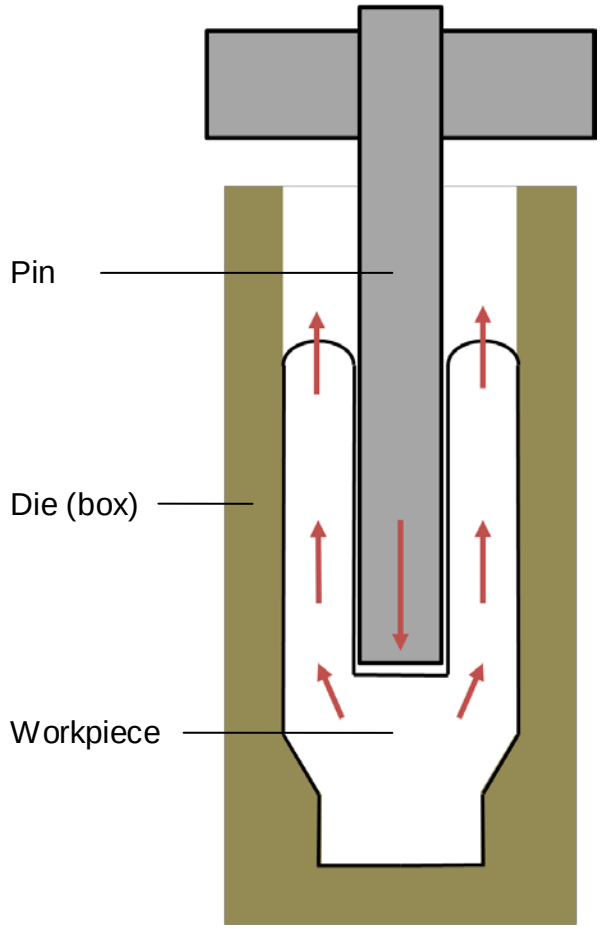


Figure 1-3. Extrusion process.

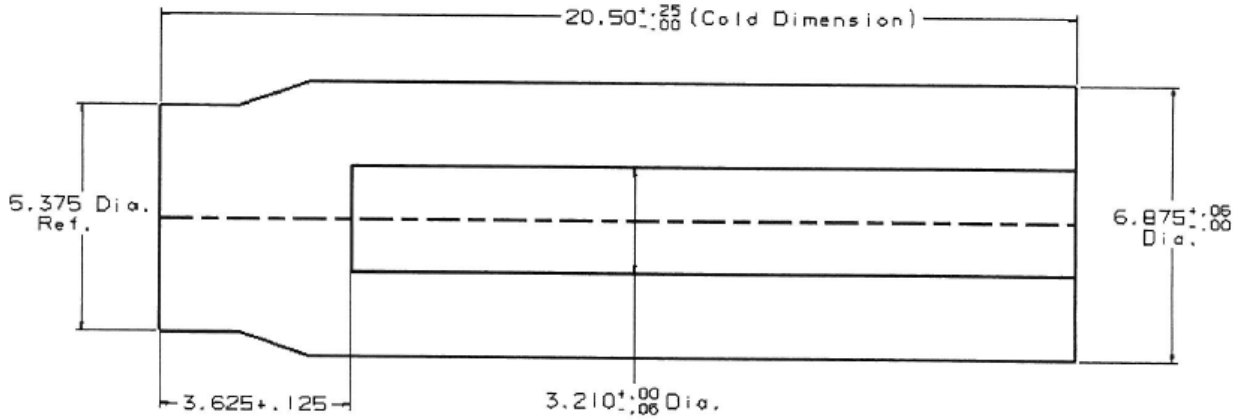


Figure 1-4. Forged tool joint dimensions before machining (inches) [1].

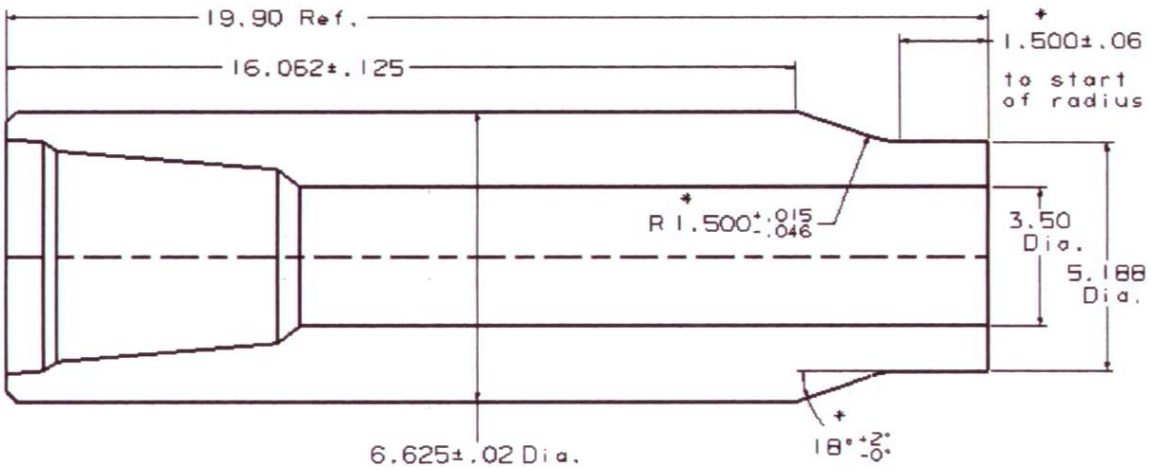


Figure 1-5. Final part dimensions (inches) [1].

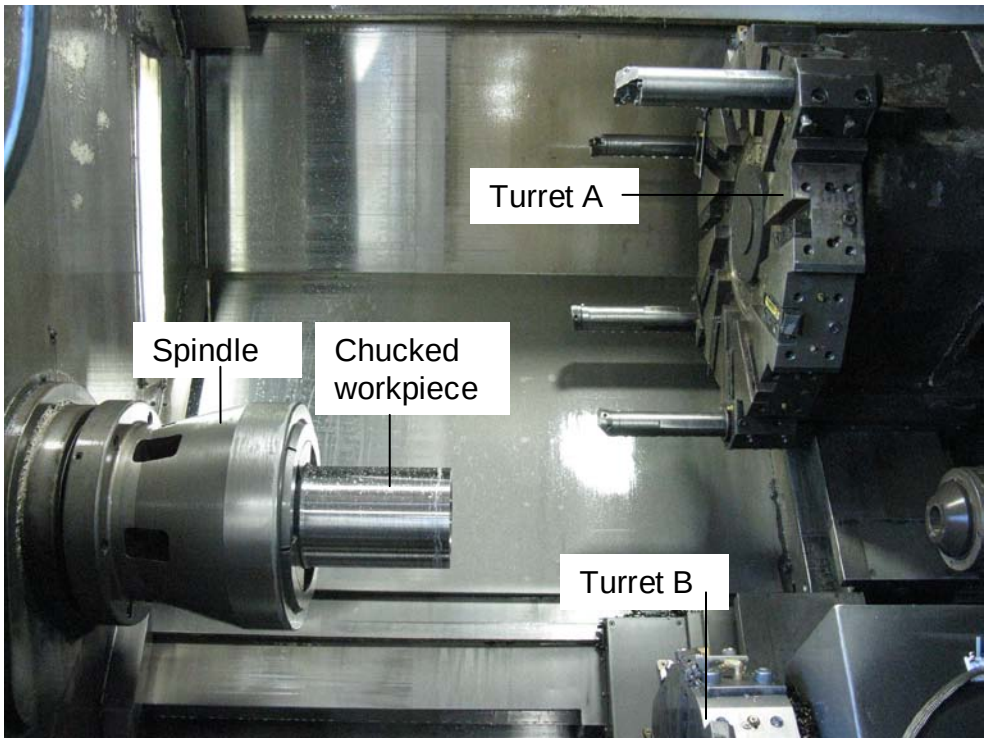


Figure 1-6. Okuma LC-40 lathe [1].

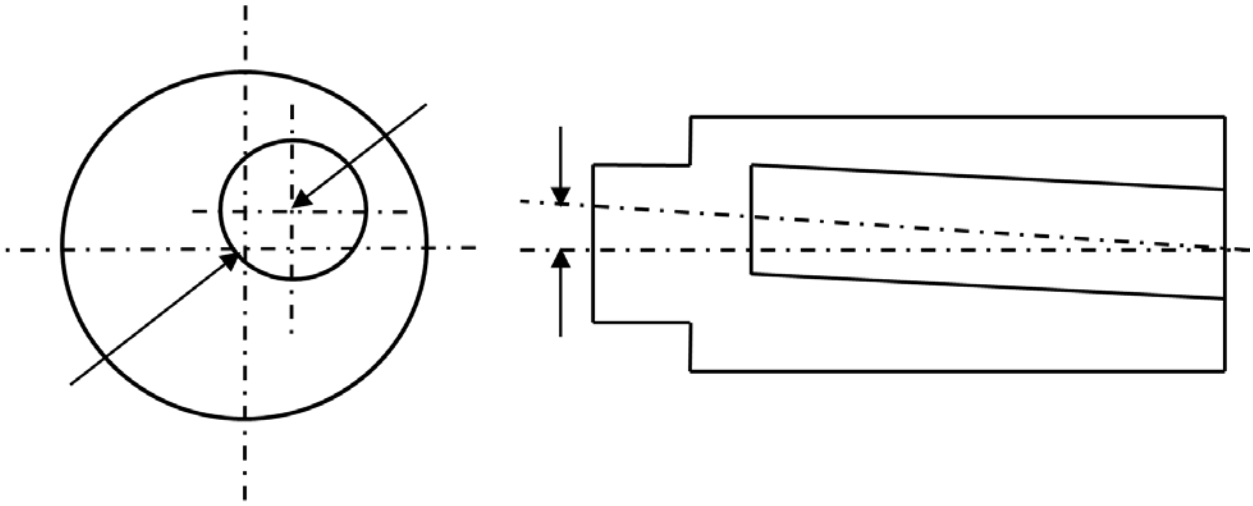

Figure 1-7. Concentricity problem .

# CHAPTER 2
# LITERATURE REVIEW

The primary method of addressing dimensional inaccuracies prior to machining is through manual inspection (statistical sampling). Manual inspection, however, adds significantly to the time and cost of producing a part since it typically requires the part to be transported to a separate location for measurement. Additionally, statistical sampling does not ensure that all defective parts are identified. The only way to ensure 100% quality control is to inspect every part. One approach used to satisfy this 100% inspection requirement in a timely manner is to inspect parts while they are chucked or clamped in the machine. Yandayan and Burdekin [2] provide a review of the different methods used to accomplish this task (up to 1996) and Vacharanukul and Mekid [3] continue the survey through 2003, but both stop short of providing a practical method for industrial applications. Six measurement groups are discussed, including mechanical, optical, ultrasonic, pneumatic, electrical, and temperature detection methods.

A popular mechanical method is the friction/roller system composed of a roller in contact with the workpiece's outer surface. As the workpiece rotates, so does the roller and an encoder tracks the roller rotation per spindle rotation in order to calculate diameter [2]. This method however, is known to cause measurement errors and its accuracy is limited [3]. Touch probes are perhaps the most common devices implemented in CNC machines and can be used to measure workpiece location/dimensions using the machine scales. The disadvantage is that measurements can only be performed at a finite number of locations. This limitation, coupled with the probe's sensitivity and expense, make taking continuous measurements to determine

part dimension prior to and after machining impractical. Many optical methods are discussed that use light directed at the workpiece and collected by a CCD camera or photodiodes to analyze the workpiece dimension [3]. While these methods are typically more robust and accurate than other methods, they are expensive, often take up too much space in the machine, and require a dry environment. Ultrasonic methods use wave propagation through the workpiece to analyze the change in the sound distribution based on the workpiece dimension. Sensor setup is complicated, requiring mirrors and detectors positioned in precise locations. Pneumatic methods apply pressure on the workpiece as it rotates and measure the dimensions based on the change in backpressure. This type of sensor is only used to measure average dimensional error due to its limited maneuverability [3], however, and requires a constant distance to be maintained between the nozzle and workpiece [2]. Electrical methods employ electrical fields created on the workpiece to measure changes in reluctance or capacitance. However, these methods are limited to measuring parts that are electromagnetic or conductive. Temperature detection methods are also implemented to measure thermal expansion of the tool that often causes diametral errors in turning. This method does not directly measure parts, but rather improves part accuracy by removing an inherent error associated with turning [2].

These are post-machining measurements used for final part verification, although they may also serve as in-process measurement completed prior to performing a finishing pass. They have not been widely applied to the pre-machining measurement of forgings for final machining operations. This is partially due to the fact that forged workpieces often have rough surfaces with pits and protrusions that can skew the

measurements and/or damage the sensors. The goal of this study, however, is to determine the complete part geometry as accurately as possible prior to machining in order to reduce machining time and chatter. Therefore, new sensors are developed to enable measurement of the required dimensions.

The geometric variations discussed in Chapter 1 cause varying chip width, *b*, during boring operations as seen in Figure 2-1. As the workpiece rotates, the depth of cut changes. If the corresponding chip width exceeds the limit stable machining conditions, self-excited vibration (or chatter) can occur. In this case, there is a feedback mechanism between tool vibrations and force. Any small perturbation can cause a change in the chip thickness. Subsequently, the force acting on the tool varies and induces a vibration of the tool. This vibration leaves behind a wavy surface, which the tool will encounter in the next revolution and again causes chip thickness variation, which leads to additional vibrations [4]. This process is termed regenerative chatter and is undesirable in turning due to the varying forces on the tool and undulated workpiece surface. These forces can cause tool failure and/or damage to the machine [5]. By measuring workpiece dimensions prior to machining, the part program can be updated to account for the actual forging geometry.

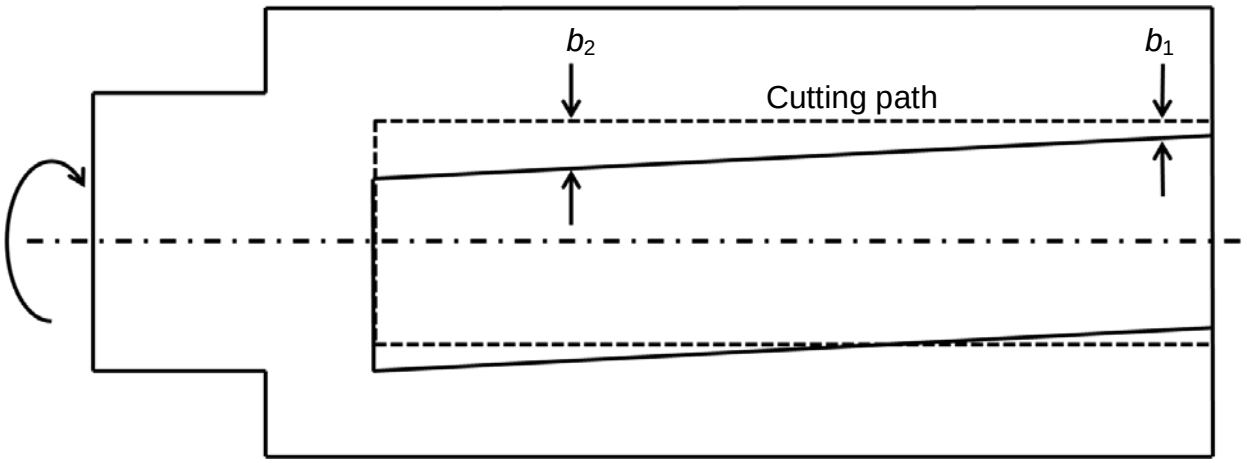

Figure 2-1. Chip thickness variation.

# CHAPTER 3
# EQUIPMENT DESIGN

In order to perform the measurements identified in Chapter 1, a linear variable differential transformer (LVDT)-based design was chosen for the probe. An LVDT design was selected due to its infinite resolution (before digital sampling), compactness, and relatively low cost. LVDTs consist of a transformer and an iron core armature. The transformer is composed of three coils: a center primary coil and two secondary coils on either side. The iron core slides through the transformer. As current is supplied to the primary coil, a voltage is induced in the secondary coils that is linearly proportional to the position of the sliding core [6]. The lack of a physical contact between the core and transformer results in infinite resolution, low noise data, and increased lifetime. The LVDT chosen for this application was the RDP Electronics DCTH300AG model transducer [7]. This series was chosen because it consisted of built-in electronics that enable a dc supply and dc output, simplifying the required electronics. The particular model chosen outputs voltage from 0 to 10 volts.

Since the workpiece is chucked on the outside surface, there are only three measurements that must be performed in order to fully define the workpiece: length, inside diameter, and the concentricity of the hole with respect to the outside diameter (the outer diameter is considered an accurate and known value based on the shop floor experience). The length measurement is completed by contacting the face of the workpiece with an LVDT probe. The other two measurements require contact with the inner diameter of the hole in the workpiece. Because a perpendicular contact measurement with the LVDT is not possible due to the small hole size and typical LVDT lengths, a small device was needed to transfer the surface normal of the inside diameter

90° onto the part/spindle axis, where it was convenient to orient the LVDT axis. A parallelogram leaf-type flexure and 45° surface was chosen to accomplish this task. Figure 3-1 demonstrates the concept behind this system. The downward displacement, y, of the platform caused by the variation in the surface is transferred to the sensor probe, x, via the 45° surface. This one-to-one ratio is maintained due to the nature of the parallel leaf-type flexure. Parasitic motion due to the shortening of the flexure arms can be calculated through substitution of Equations 3-2 through 3-4 into Equation 3-1 and proved to be insignificant [8]. For a maximum expected deflection of 11 mm, the parasitic motion is calculated to be 0.01 µm.

$$y = \left( \frac{x^3\left[\frac{M_1}{6\mathrm{L_p}}(\mathrm{k}-2)\right] + x^2\left[\frac{M_1}{2}(1-\mathrm{k})\right] + x\left[\frac{M_1 \mathrm{L_p}}{6}(2\mathrm{k}-1)\right]}{-\mathrm{E_p I_p}} \right) \tag{3-1}$$

$$M_1 = \frac{F \mathrm{L_f}}{4} \tag{3-2}$$

$$F = \frac{24 \mathrm{E_f I_f}}{\mathrm{L_f}^3}\,\delta \tag{3-3}$$

$$\mathrm{k} = \frac{4\mathrm{s}}{\mathrm{L_f}} \tag{3-4}$$

- $E_p$ is Young's modulus of the platform
- $I_p$ is the area moment of inertia of the platform
- $y$ is the parasitic motion
- $x$ is the point along the platform where parasitic motion is being calculated ($L_p/2$)
- $\delta$ is the deflection (maximum expected value was 11 mm)
- $M_1$ is the bending moment at the end of the platform
- F is the applied force per unit length (maximum expected value was 60 N)
- $E_f$ is Young's modulus of the flexure arm
- $L_f$ is the length of the flexure arm
- $L_p$ is the length of the platform or distance between flexures
- k is a correction factor for the distance between where load is applied and where deflection occurs
- s is the distance between applied load and the flexure arm
- $I_f$ is the area moment of inertia of the flexure arm

## Length Probe Design

It was found through experimentation that any side loading on the LVDT resulted in significant noise and error. For this reason, a shaft supported by bearings was implemented in the design to take any side loading from the rough surface of the workpiece and transfer only axial motion to the LVDT. The shaft is supported by two linear ball bearings and the LVDT is supported by two collars. Both are secured inside an aluminum tube. This ensures that both shaft and LVDT share (nominally) the same motion axis. A hardened (harder than workpiece) stainless steel precision ball is fixed to the end of the shaft and is the part that actually makes contact with the workpiece in order to limit scratching or wear of the instrument. The shaft is preloaded against the workpiece by means of a spring, and the LVDT is preloaded against the other end of the shaft through its own internal spring. A collar is fixed to the right end of the shaft to resist the spring preload and hold it in place when it is not in contact with the workpiece. See Figure 3-2 . An exploded view of the entire design is shown in Figure 3-3. The complete assembly is mounted onto the top turret (turret A) on a boring block holder; see Figure 3-4. This ensures that the axis of symmetry of the assembly is coincident with the z axis of the machine and also that the tip of the probe has a zero offset in the x direction.

## Concentricity Probe Design

A separate device was needed for measuring the inside diameter of the workpiece. As discussed previously, in order to transfer motion from the diametral x direction to the z (part/spindle) axis, a parallelogram, leaf-type flexure was used. Figure 3-5 shows the concentricity probe design; Figure 3-6 and Figure 3-7 provide additional details. The only difference between this design and the length probe design is the

addition of the flexure and platform to the end that contacts the workpiece. The platform has a hardened stainless steel precision ball attached to its top for maintaining contact with the workpiece. As the workpiece rotates, the hole's radial error motion (due primarily to an offset between its center and the spindle axis, which is assumed to be coincident with the center of the workpiece's outer diameter) causes the inner surface to push against the platform and deflects the flexure in the x direction. The x displacement is transferred to the shaft's z axis through the 45° machined surface on the platform. The LVDT is preloaded against the other end of the shaft and measures this z motion. Another hardened precision ball is attached to the left end of the shaft and maintains contact with the 45° face. To reduce friction and abrasion at the 45° surface, a thin piece of glass was epoxied to the 45° surface.

## Completed Sensors

Table 3-1 lists all parts that were either purchased or manufactured including all electronics necessary for this project.

In order to convert all the LVDT voltages into the appropriate measurements, the raw data must first be recorded and saved for post-processing. National Instrument's LabVIEW software was chosen for this task. The voltage from the LVDT is recorded as a function of time by the software. This data, in addition to other variables specific to the current measurement (measurement type, location, calibration constant, etc.) is saved as an .lvm file. The hardware required to accomplish this task include the LVDT, an ac-dc power supply, a data acquisition board (DAQ), a connector block, and a laptop computer. The voltage from the LVDT is already pre-processed to enable a dc supply and dc output so the output voltage passes directly through the connector block via a feed through input module to the DAQ and then from the DAQ to the laptop via USB.

The setup is shown below in Figure 3-8. The fully assembled devices are shown in Figure 3-9 and Figure 3-10. The program used to save this data is provided in Appendix A. The post processing is accomplished by MATLAB and the accompanying code is provided in Appendix B.

Table 3-1. Parts list.

| Part Description | Material Description | Quantity | Total Cost |
|---|---|---|---|
| Tube | 2024 Aluminum | 1 | $54.36 |
| LVDT shaft collar | 316 Stainless Steel | 4 | $61.52 |
| Precision shaft | AISI 1566 Rockwell C60 | 1 | $29.34 |
| Linear ball bearing | 440c Stainless Steel | 4 | $182.72 |
| Retaining ring | PH 15-7 MO Stainless Steel | 1 | $7.87 |
| Flexure leaf | 430 Stainless Steel | 1 | $6.75 |
| Boring bar | 6061 Aluminum | 1 | $26.25 |
| Grade 24 3/8" ball | 440c Stainless Steel Rockwell C58-C65 | 1 | $4.51 |
| Grade 100 1/2" ball | 440c Stainless Steel Rockwell C58-C65 | 1 | $14.62 |
| Cylinder base | 6061 T651 Aluminum | 2 | $150.00 |
| Flexure platform | 304 Stainless Steel | 1 | $95.00 |
| Spring support | 6061 T651 Aluminum | 2 | $30.00 |
| Spacer | 6061 T651 Aluminum | 2 | $40.00 |
| Top | 304 Stainless Steel | 2 | $320.00 |
| Flexure clip | Aluminum alloy | 4 | $0.00 |
| Hard stop | Aluminum alloy | 1 | $0.00 |
| Spring | Steel alloy | 2 | $1.08 |
| No. 4 washer | 18-8 Stainless Steel | 1 | $1.60 |
| 4-40 screws | 18-8 Stainless Steel | 1 | $2.84 |
| 3/8"-24 screws | 18-8 Stainless Steel | 2 | $5.76 |
| 5/16"-24 screws | 18-8 Stainless Steel | 1 | $8.27 |
| 10-32 set screws | 18-8 Stainless Steel | 4 | $2.72 |
| LVDT | N/A | 2 | $1,030.00 |
| Power supply | N/A | 1 | $124.00 |
| USB DAQ-6289 | N/A | 1 | $2,339.10 |
| Shielded cable | N/A | 1 | $89.10 |
| Connector block | N/A | 1 | $359.10 |
| Feed through input | N/A | 1 | $44.10 |
| Laptop | N/A | 1 | $1,484.41 |
| Total | | | $6,515.02 |

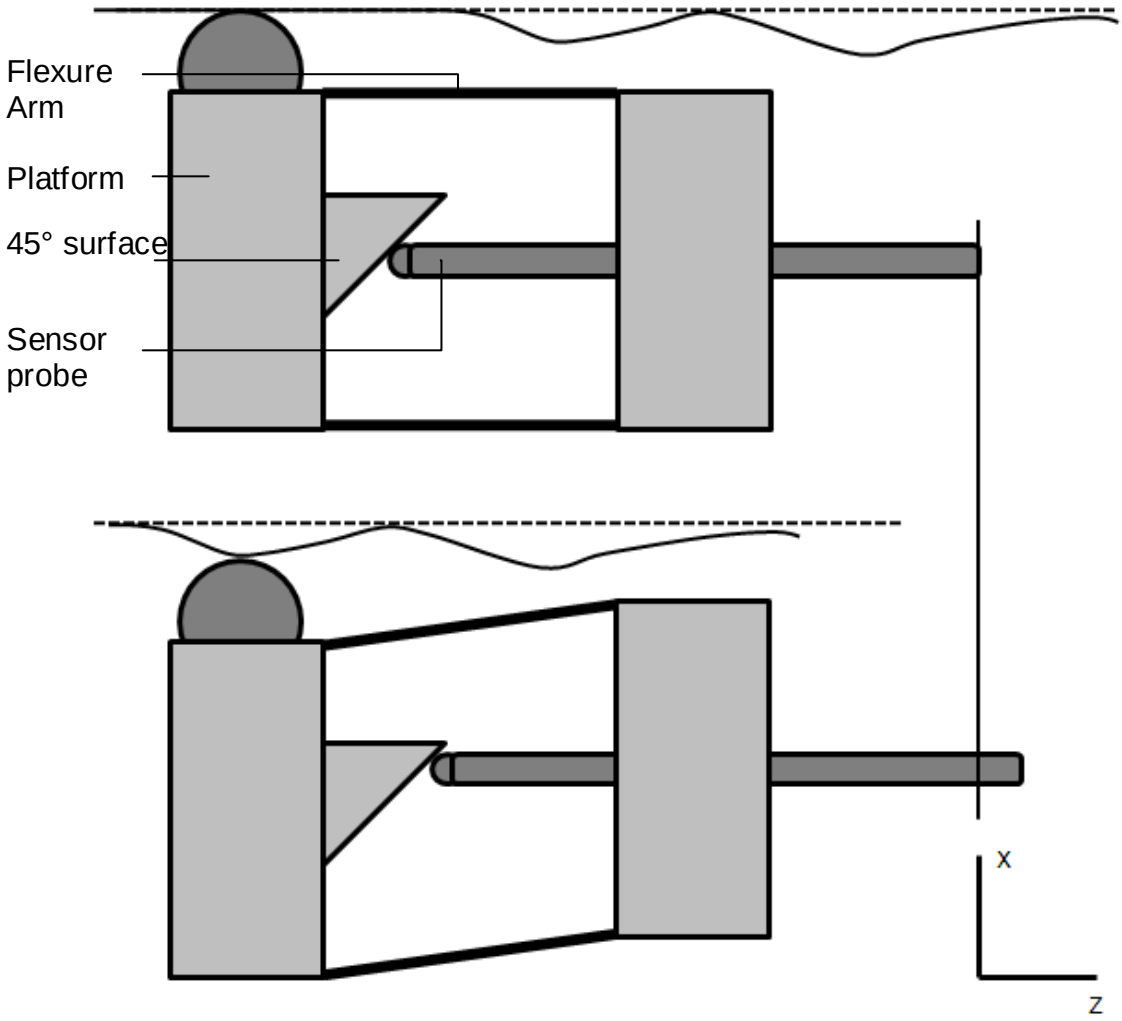


Figure 3-1. Flexure concept.

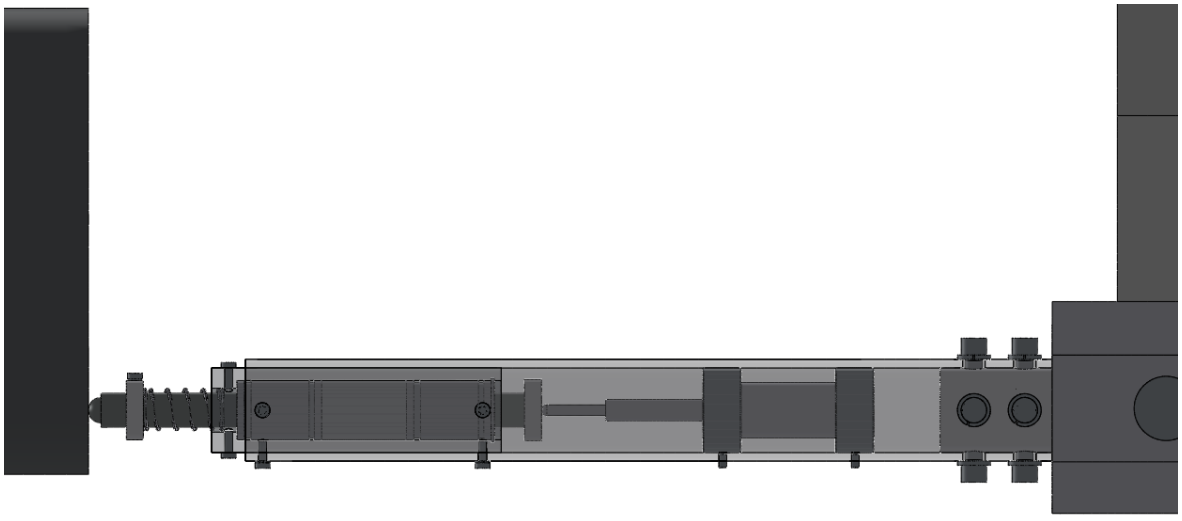

Figure 3-2. Length probe design.

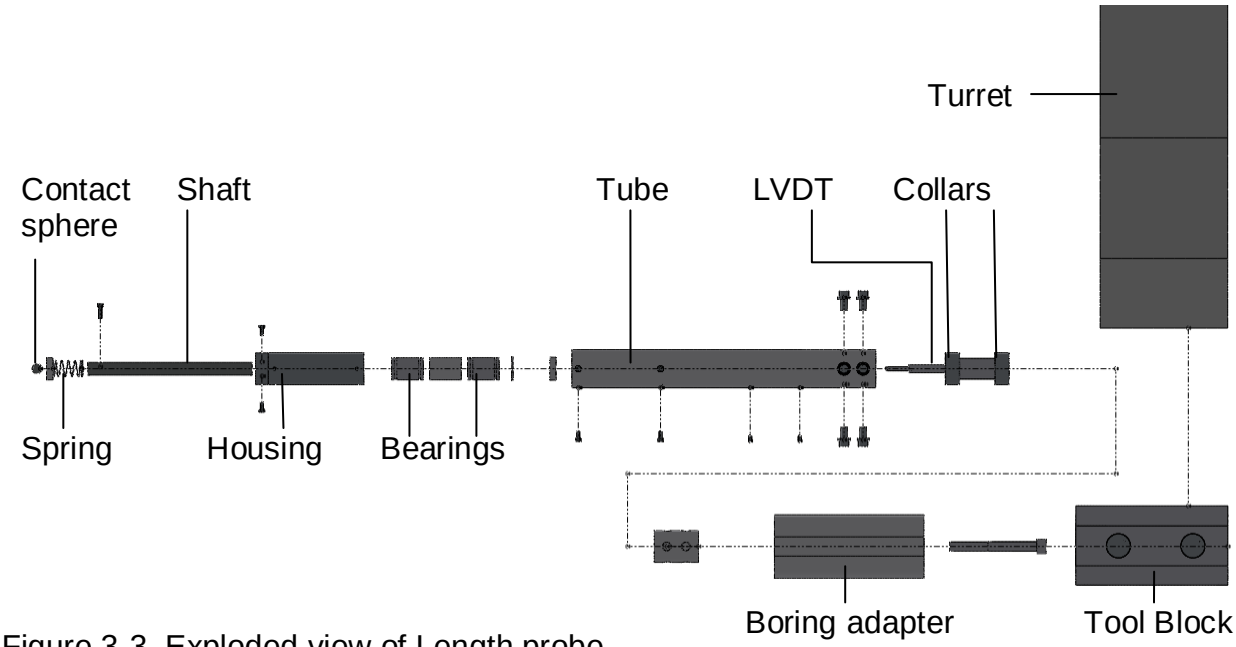


Figure 3-3. Exploded view of Length probe.

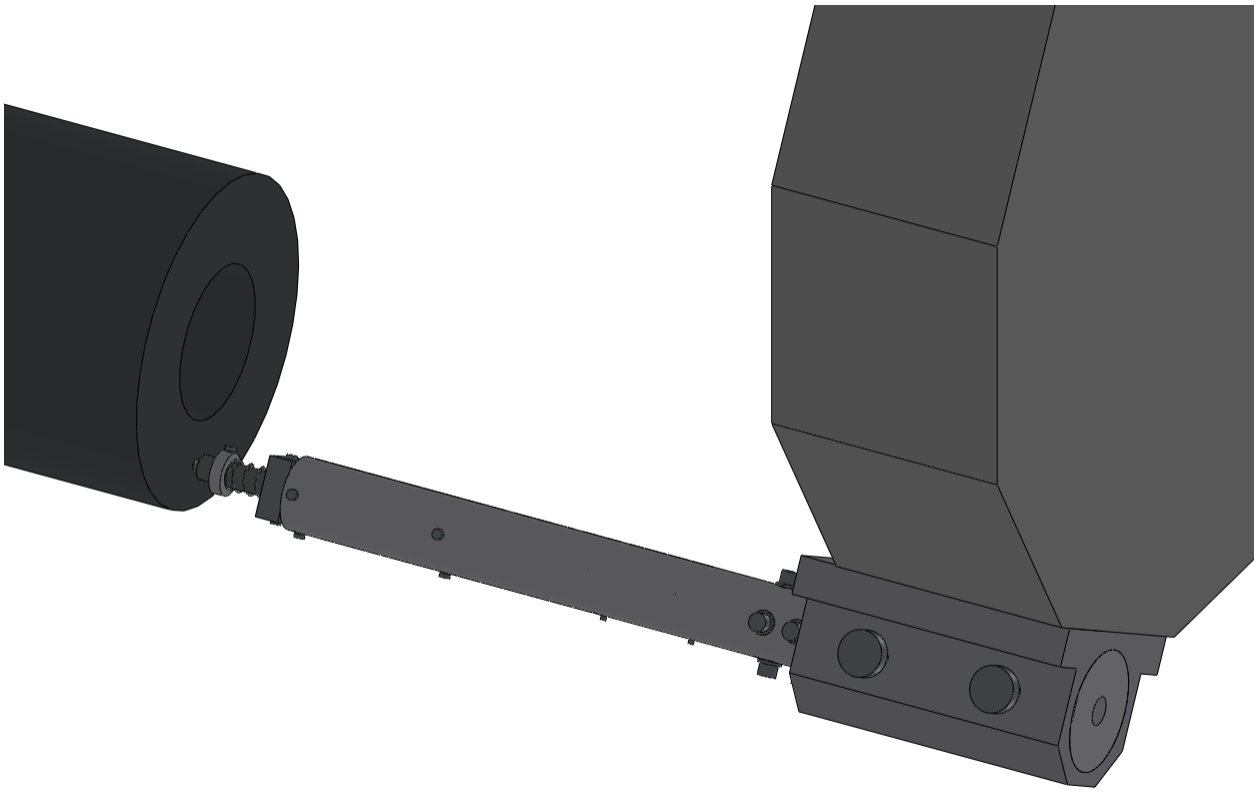

Figure 3-4. Length probe mounted on turret.

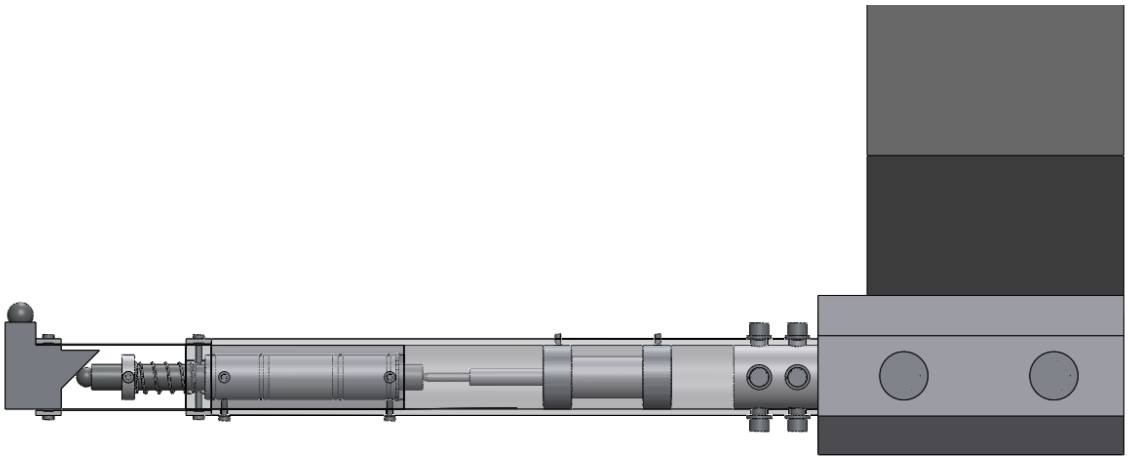

Figure 3-5. Transparent side view of concentricity probe.

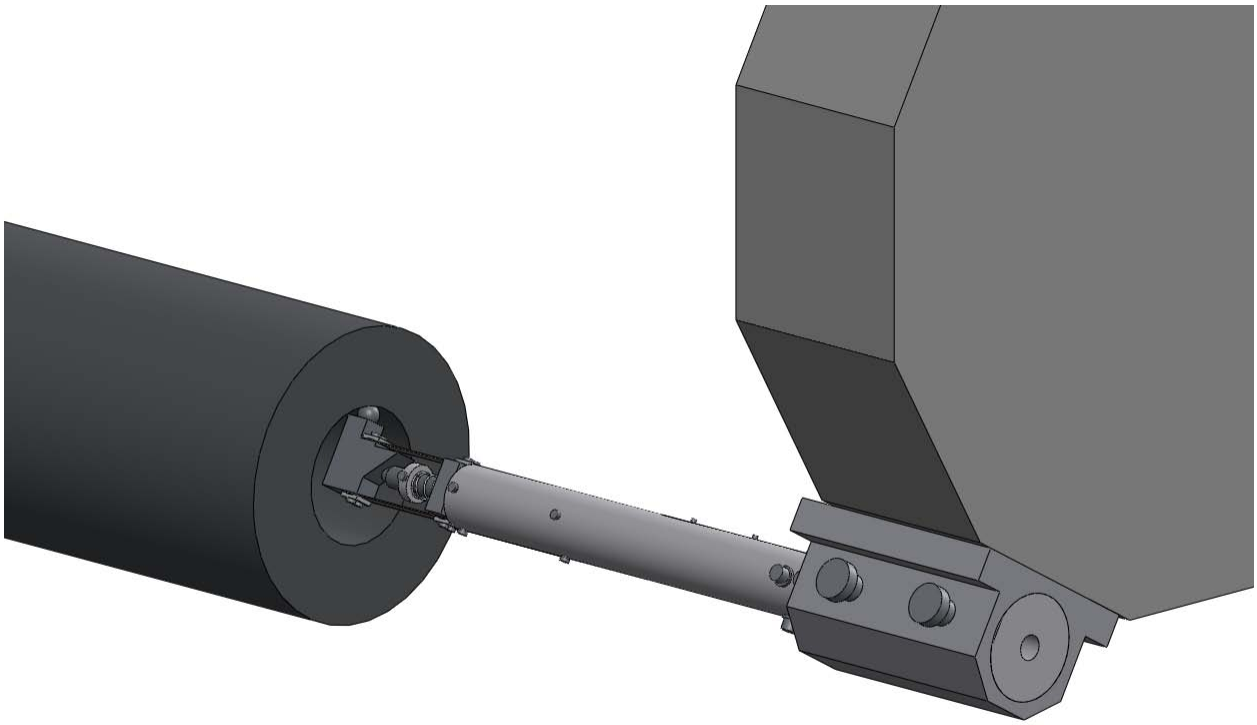

Figure 3-6. Concentricity probe.

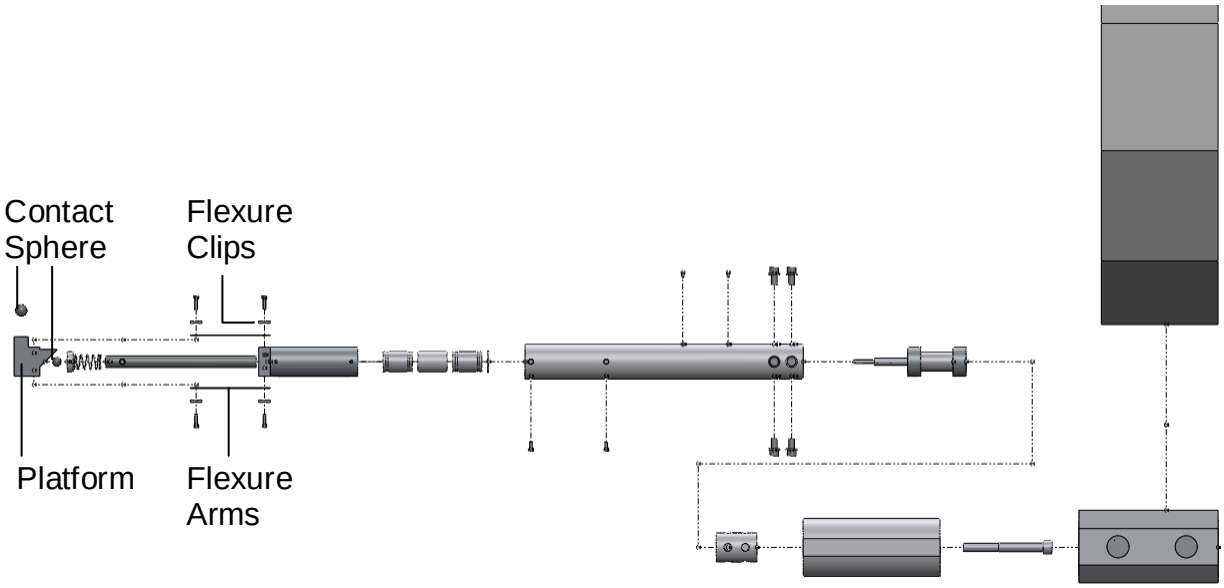


Figure 3-7. Exploded view of concentricity probe.

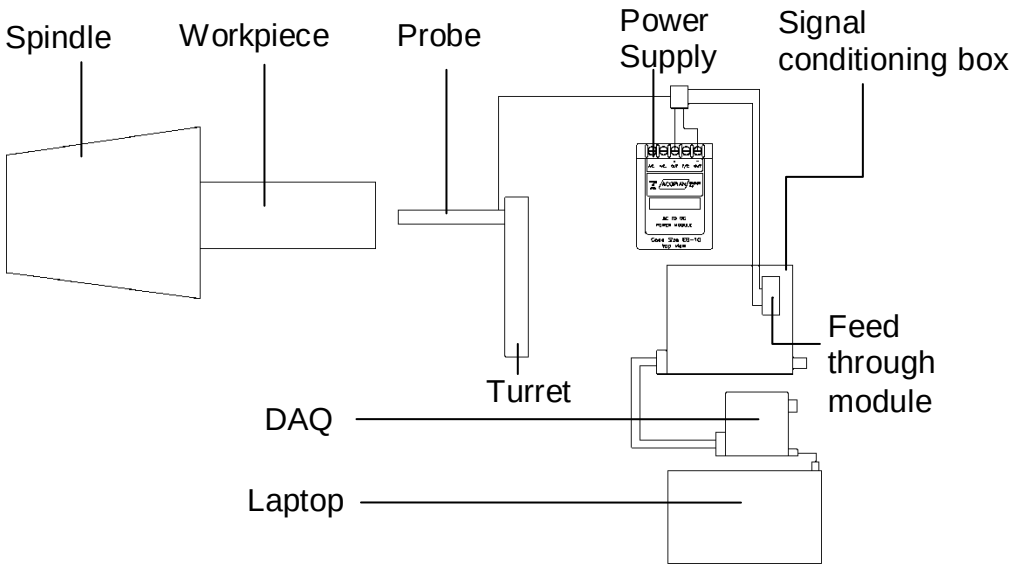


Figure 3-8. Electronic setup.

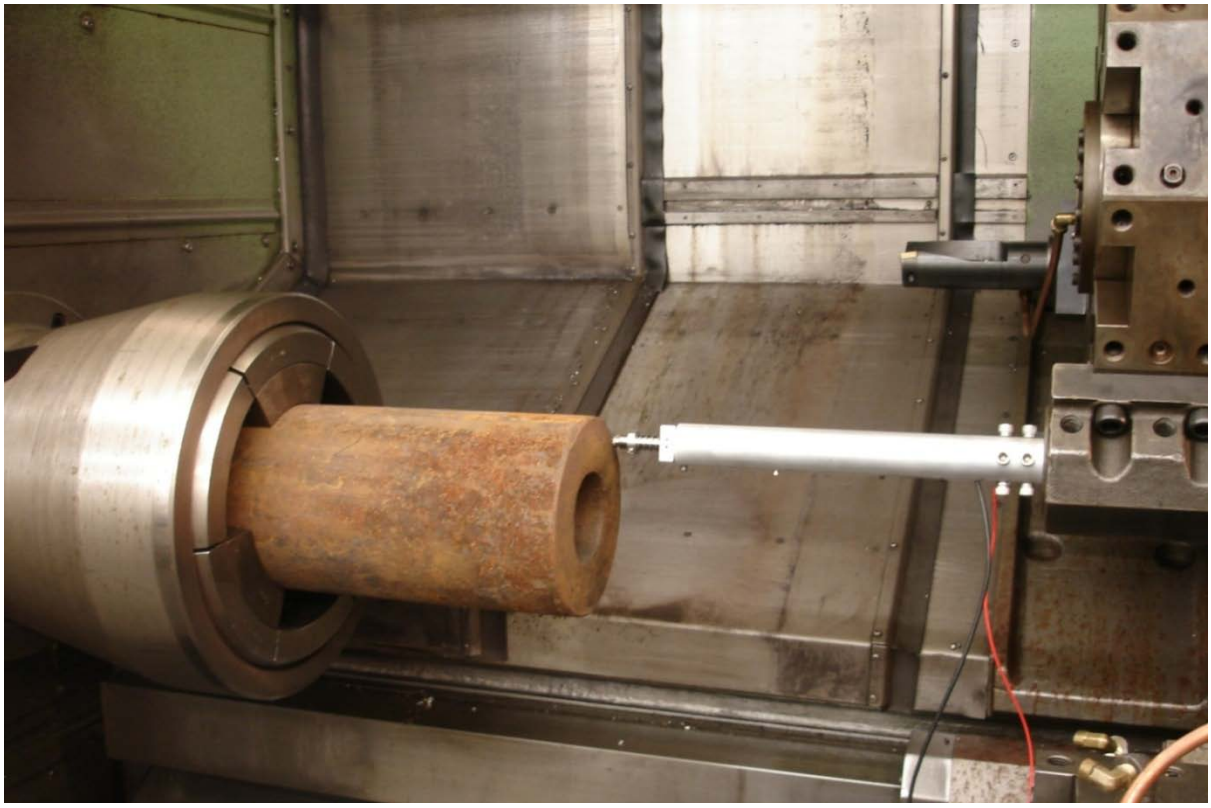

Figure 3-9. Length probe on Okuma LC-40 lathe.

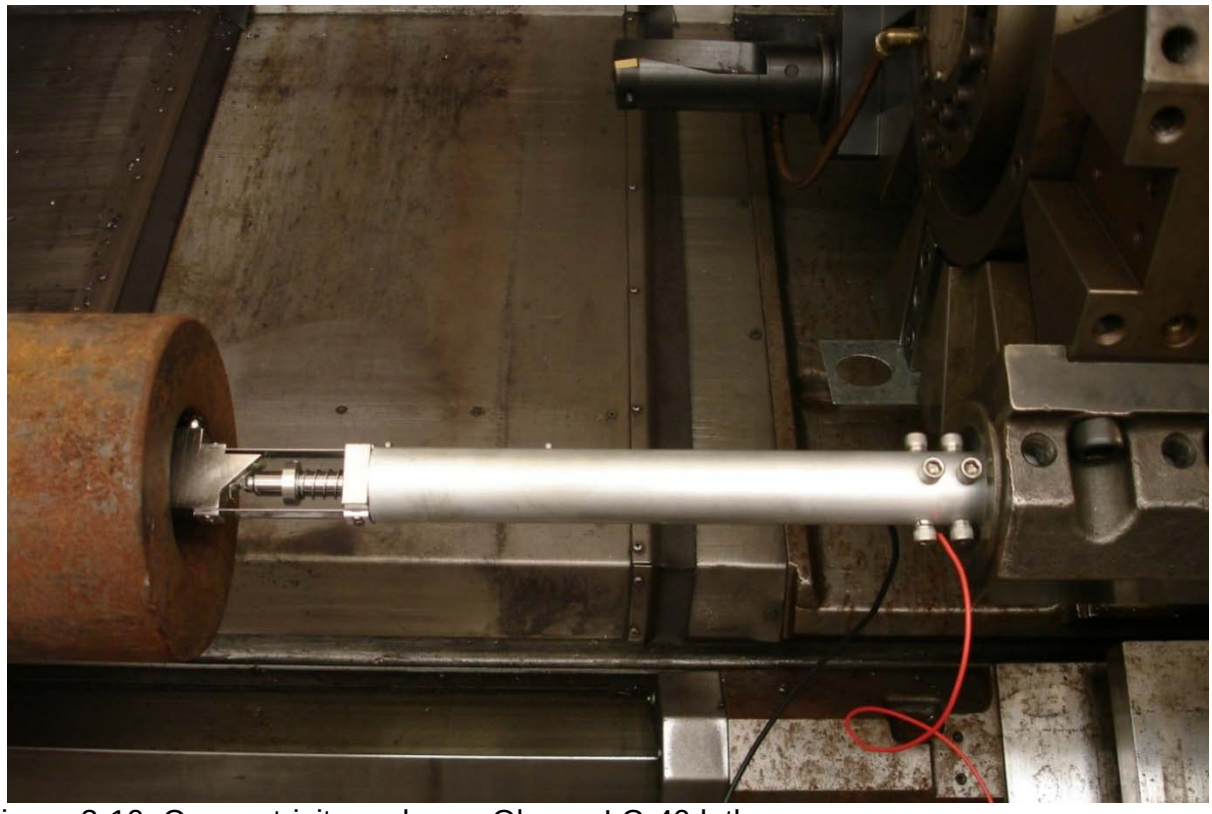

Figure 3-10. Concentricity probe on Okuma LC-40 lathe.

# CHAPTER 4
# EXPERIMENTAL PROCEDURE

## Bench Top Tests

The devices were initially tested in a controlled environment to ensure proper functioning before measuring actual workpieces on a lathe. Numerous bench top tests were performed with the devices fixed to a vibration isolation table in a temperature controlled room maintained at 20 °C. For these initial tests, the contact ball was placed in contact with a single axis micrometer stage. The stage was then moved in different increments and the output voltage was recorded.

The noise of the data throughout all tests ranged from ±14 to ±23 mV. This is in accordance with the manufacturer's rating of a maximum of ±25 mV noise range. Due to the presence of noise, average values of voltage were used for static measurements. In a first experiment, the voltage was recorded every 0.5 mm up to 2 mm and then back to 0 mm. Using the manufacturer's calibration constant of 0.65028 V/mm for the length probe, the results for the length probe were accurate to within +1 / -2 µm when compared with the motion stage micrometer. Since the manufacturer lists an uncertainty in the calibration of 4.2 µm, these results were considered acceptable. An additional experiment was conducted to evaluate device hysteresis. In this case, the sequence of commanded displacement was {0, 1, 3, 1, 0, 3, 1, 3, 0} mm. Values for the length probe were accurate to within +0 / -11 µm. No significant hysteresis was observed; a maximum difference of 2 µm was measured between the forward and reverse motions.

The concentricity probe experiments were performed next. The first test yielded results that did not agree with the stage encoder when using the manufacturer's calibration constant of 0.65153 V/mm. Calculated displacements were off by as much

as 300 µm. However, the results were repeatable, suggesting that reasonable results were possible if a different calibration constant were to be applied. Using a least square fit, a new calibration constant was calculated to be 0.61123 V/mm. Using this new calibration constant, results agreed to within +0 / -20 µm. The hysteresis test demonstrated that there was hysteresis in the design. Typical values ranged from 28 µm to 84 µm with higher values occurring during larger deflections (5 mm) of the flexure. For diametric part tolerances within 3 mm, the corresponding hysteresis values for this amount of deflection ranged from 30 µm to 50 µm. Using the new calibration constant, the largest differences from micrometer readings were found to be +57 / -23 µm. Given a maximum noise range of ±23 mV and the new calibration constant of 0.61123 V/mm, a measured displacement has an uncertainty range of ±38 µm so the stage displacement measurement results are acceptable.

### Alignment Errors

It is believed that the primary source of disagreement between the stage micrometer and sensor displacement is due to misalignments during device assembly and between the device and the micrometer stage axes. A comprehensive explanation of each error is provided in the following paragraphs. In these error descriptions, $\Delta Y$ is the displacement of the micrometer (the commanded displacement) and $\Delta X$ is the measured displacement of the LVDT probe using the manufacturer's calibration constant. Based on all bench top tests for the concentricity probe, the average ratio of $\Delta X$ to $\Delta Y$ was found to be 0.989. The length probe's ratio was found to be 0.999. Since the concentricity probe had a greater disparity between commanded and measured displacements, the following error discussion focuses on its design.

The first error is associated with alignment between the micrometer stage axis and the probe axis. Since this setup was fixed with screws using visual inspection, the associated cosine error must be considered. Figure 4-1 demonstrates this alignment problem. If ΔY was equal to ΔX then the angle α would be zero and ΔX would transfer the micrometer motion to the rest of the device precisely (assuming all other alignments were perfect). Since the ratio of ΔY to ΔX is actually 0.989, then if all other alignments are perfect, this angle would have to be 8.5° in order to fully account for the error seen in the bench top tests.

The second type of alignment error would occur if the platform was misaligned at the angle shown in Figure 4-2. If this were to occur, then the contact between the shaft (assumed here to be perfectly aligned with the LVDT axis) and the 45° surface would follow a different path (ΔX instead of ΔY). This also produces a cosine error and its magnitude would have to be 8.5° if it were the only misalignment in the setup.

The third alignment error depends on the accuracy of the 45° surface of the platform. If this angle deviates from 45°, then a tangent error is present. This error has greater implications in the overall error of the device. An angle that deviates by only -0.32° from 45° would be necessary if this was the only alignment error. See Figure 4-3.

Another alignment error associated with the platform is if the holes drilled on top and bottom were not axisymmetric. This would cause a twist of the platform, resulting in a shift in the angle of the 45° surface; see Figure 4-4. This produces a second tangent error, and it also would require an angle of -0.32° to fully account for the entire misalignment of the device.

The last alignment associated with the platform produces the final tangent error. If the lengths of the arms of the flexures are not equal, it would again cause a twist of the platform resulting in the same error described previously. Although it is believed that the lengths are the same (they were drilled on a CNC machine), there still exists a tolerance between the clearance holes and the screws used to hold them in place. It is most likely this factor that twists the platform due to different arm lengths and may produce an additional alignment error.

The sixth error comes from the potential misalignment of the shaft with the platform. This may be due to numerous variables including the fit between the shaft and bearings, the alignment between the bearings and the housing and/or the alignment between the housing and the tube. Any one of these may cause the shaft to not be perpendicular to the platform and therefore cause a cosine error. Again this misalignment would have to be 8.5° in order for it to be the single error. See Figure 4-5.

The last error involved in the design depends on the alignment of the LVDT shaft with the rest of the setup. Similar to the previous error, the two shaft collars for the LVDT may not be holding the LVDT coaxially with respect to the tube. This would also require a cosine error of 8.5°. See Figure 4-6.

Choosing appropriate values for each potential misalignment, a check can be made to see if the ΔX / ΔY ratio can be attributed to misalignment. An appropriate, conservative, value for any of the four cosine errors in this design is chosen as ±0.5° yielding a ΔX / ΔY ratio of 0.9999. Since the 45° surface has a tolerance of ±0.05°, the first tangent error takes a value 0.998. The second tangent error also uses the tolerance during manufacturing to achieve a tangent error value of 0.994. The difference between

the screw diameter and a close fit clearance hole is 0.1 mm. Given the distance between the holes and assuming a worst case scenario, this would rotate the platform by 0.36° yielding a ratio of .987 for the last tangent error. Multiplying all these errors together yields a ΔX to ΔY ratio of 0.979 which is lower than the experimental value. This suggests that the discrepancy between commanded displacement and measured displacement might be attributed to alignment errors within the design.

**Procedure for Length Probe Measurements**

The bench top tests showed that the devices were capable of acceptable measurement accuracy provided a compensated calibration constant is used to correct any misalignment in the device. For this reason, a new calibration constant needs to be determined once the devices were mounted to the Okuma lathe. This process is detailed next.

- The first step is to ensure proper connection of all wires. Data is collected while the probe is manipulated in order to check for changes in the output. The noise value is measured to ensure proper grounding.
- The turret is then moved until the probe is in contact with the lathe's backstop (see Figure 5-9) approximately at the LVDT's center of travel. The machine Z value is recorded as $Z_{ref}$ and the voltage is recorded as $V_{ref}$. Since this is a static measurement, the average voltage is used.
- The turret is moved along the Z axis in steps of 0.02" and the voltage is recorded at each discrete location up to 0.28" and then back to 0.
- The calibration constant is found by plotting voltage versus machine displacement and performing a regression analysis to identify the best fit line through the data. The slope of this line yields a constant with units V/mm (after being converted from V/in) which is used as the fixed calibration constant.

Once the probe's calibration constant was determined, the probe performance was verified using an artifact of known dimensions. The artifact is shown in Figure 4-7. This

artifact was machined and measured on a coordinate measuring machine (CMM) at the University of Florida's Metrology Laboratory to determine its length and diameters.

In order for voltage readings/displacements from the LVDT to be translated into part dimensions with values larger than the LVDT range, a referencing technique was required. The approach was to use the machine scales for macroscale motion between a reference surface and the surface to be probed. Combining this value with the difference in LVDT readings when touching the two surfaces enabled the part dimensions to be determined. The Okuma LC-40 lathe has a circular reference plate backstop located inside the collet. All workpieces when chucked in the collet are pushed against this reference plate. This reference plate was therefore chosen as the reference point for the length probe.

In order to measure the artifact with the length probe, it is chucked in the lathe and acceptable runout is verified using a dial indicator. Next the probe, which is clamped in the upper turret, is placed in contact with the face of the artifact at approximately its center of travel by adjusting the turret Z position. The machine Z value is recorded as $Z_{loc}$ and the voltage from the LVDT is recorded as $V_{meas}$. If $V_{meas}$ is the same as $V_{ref}$ then the length of the artifact can simply be calculated as the difference between the machine Z values ($Z_{loc}$-$Z_{ref}$). However, if the voltages are not the same (indicating that the probe was not moved to exactly the same distance away from the surface of the workpiece as it was from the reference plate) then this small displacement must be taken into account by either adding or subtracting it from the current machine Z position before being used to determine part length. A more detailed explanation is included in Chapter 5.

A similar process is applied for measuring actual forged workpieces. Once the workpiece is mounted and checked for proper chucking, the turret position is adjusted to move the probe into contact with the face of the workpiece near its center of travel. This is recorded as $Z_{loc}$ and, from this point forward in the measurement sequence, the machine Z value does not change. Next, the turret is moved in the X direction until the probe is near the part's outer diameter. This marks the starting point for determining the location on the face with the highest bulge. See Figure 4-8. Ten discrete measurements are completed from the outer diameter to the inner diameter. Since the voltage decreases as the LVDT pin is pressed in, the machine X value associated with the lowest voltage identifies the location where the bulge is largest. The machine is then moved to this location and this value is recorded as $X_{peak}$.

The next step is a continuous measurement around the face of the workpiece. The data acquisition program provided in Appendix A is executed and the workpiece is rotated at approximately 18 rpm. Voltage is recorded as a function of time for approximately 15 seconds. Once noise is filtered out, the lowest voltage is used together with: 1) reference voltage at the backstop; 2) the machine Z value at the backstop; and 3) the machine Z value at the face measurement location, to calculate the part's maximum length.

**Procedure for Concentricity Probe Measurements**

A similar process is used for the concentricity probe. Since the Okuma LC-40 lathe does not have a reference stop for the diametric axis, the artifact is used to determine the probe's calibration constant and reference values.

- The first step is to ensure proper connection of all wires. Data is collected while the probe is manipulated in order to check for changes in the output. The noise value is measured to ensure proper grounding.

- Next, the artifact is mounted on the lathe and runout is checked to ensure proper chucking. The spindle is locked to prevent any further motion of the artifact.
- The turret is then moved such that the probe is located inside the artifact so that the contact ball touches the first inside diameter of the artifact with the flexure deflected about half its total amount. See Figure 4-7 and Figure 4-9.
- The machine X value is recorded as $X_{ref}$. At this point, continuous data is collected using the program in Appendix A while the artifact is rotated at 18 rpm for approximately 15 seconds or four full spindle rotations. If the artifact is perfectly concentric then the voltage, $V_{ref}$, will be constant. A midrange value is used otherwise.
- The turret is moved along the X axis in steps of 0.04" and the voltage is recorded at each discrete location up to 0.16" and then back to 0. Note that the machine X scale records diameters, not displacements, so for every 0.04" displacement, the machine X value increases by 0.08".
- The calibration constant is found by plotting voltage versus machine displacement and determining the best fit line through the data. The slope of this line yields a constant with units of V/mm (after being converted from V/in) which is used as the compensated calibration constant.

In order to verify the probe performance, it is placed in contact with the second inside surface of the artifact. The machine's Z value and X value are measured as $Z_{loc}$ and $X_{loc}$. The program in Appendix A is again executed and the spindle is rotated while voltage is recorded. The references from the first surface are used to calculate the second surface diameter. The method by which voltage is converted to a dimension is explained in Chapter 5.

Workpiece measurements are conducted in a similar fashion. The probe is placed in contact with the surface of the workpiece. Both Z and X machine values are recorded and then data is collected during rotation of the workpiece. An additional three measurements are also completed at increasing depths along the inside of the workpiece. Before each measurement, the spindle is returned to the same orientation.

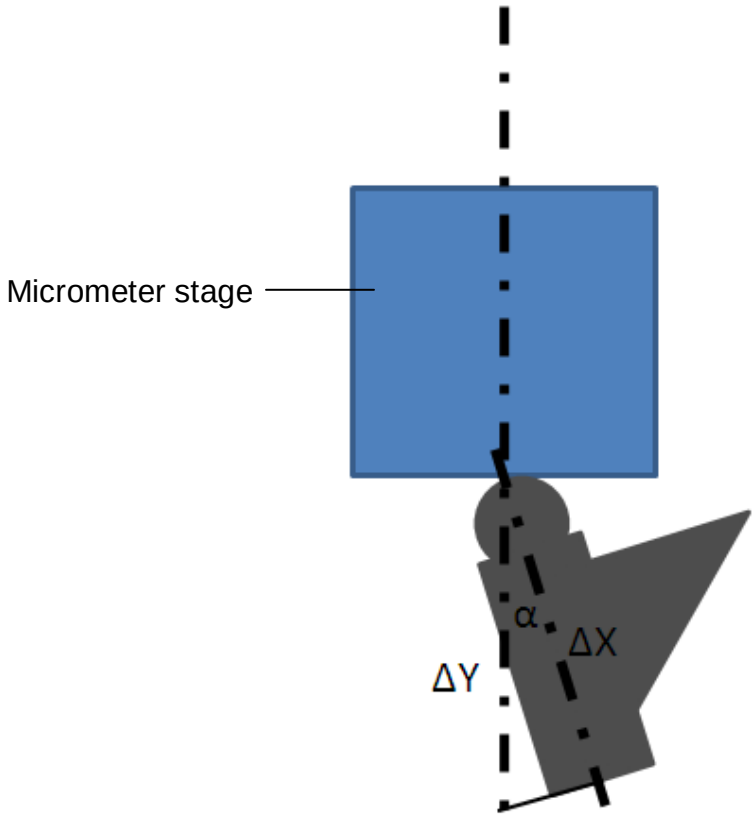


Figure 4-1. Micrometer cosine error.

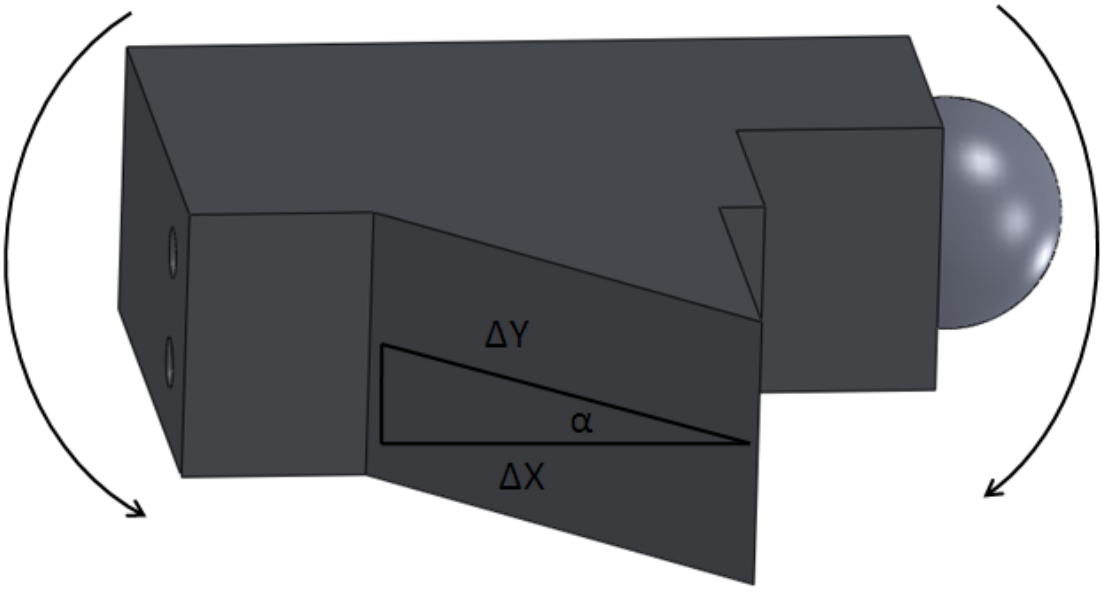


Figure 4-2. Platform cosine error.

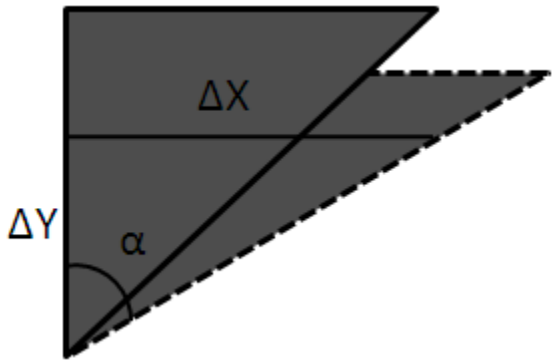


Figure 4-3. Milled surface tangent error.

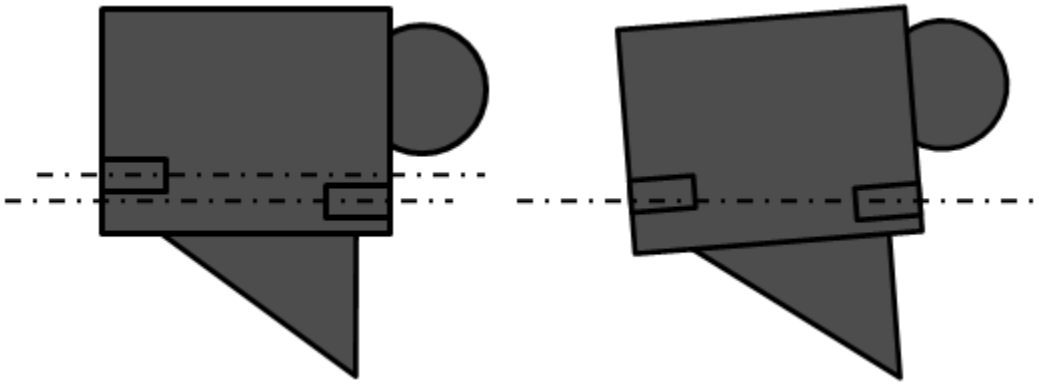

Figure 4-4. Hole tangent error.

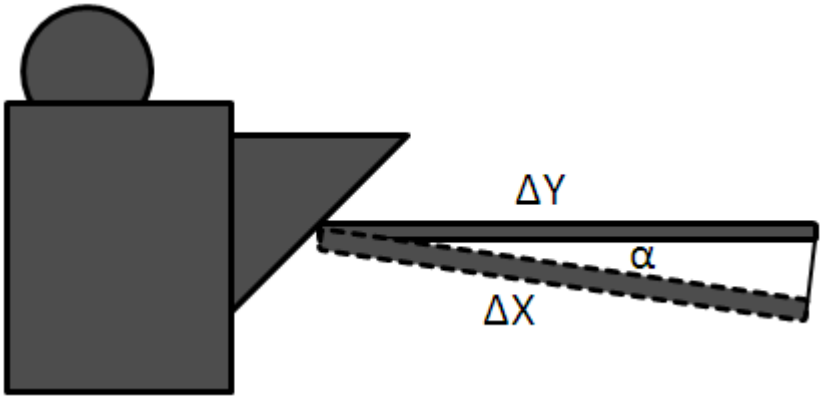


Figure 4-5. Shaft cosine error.

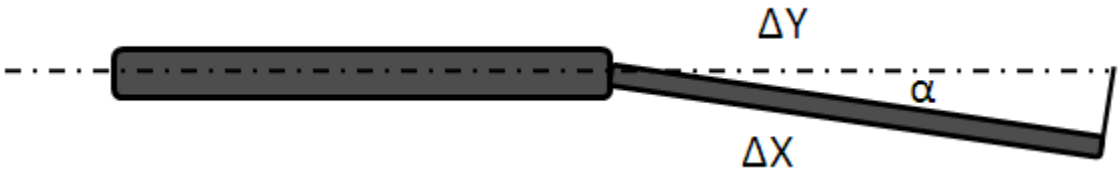


Figure 4-6. LVDT cosine error.


Figure 4-7. Artifact.

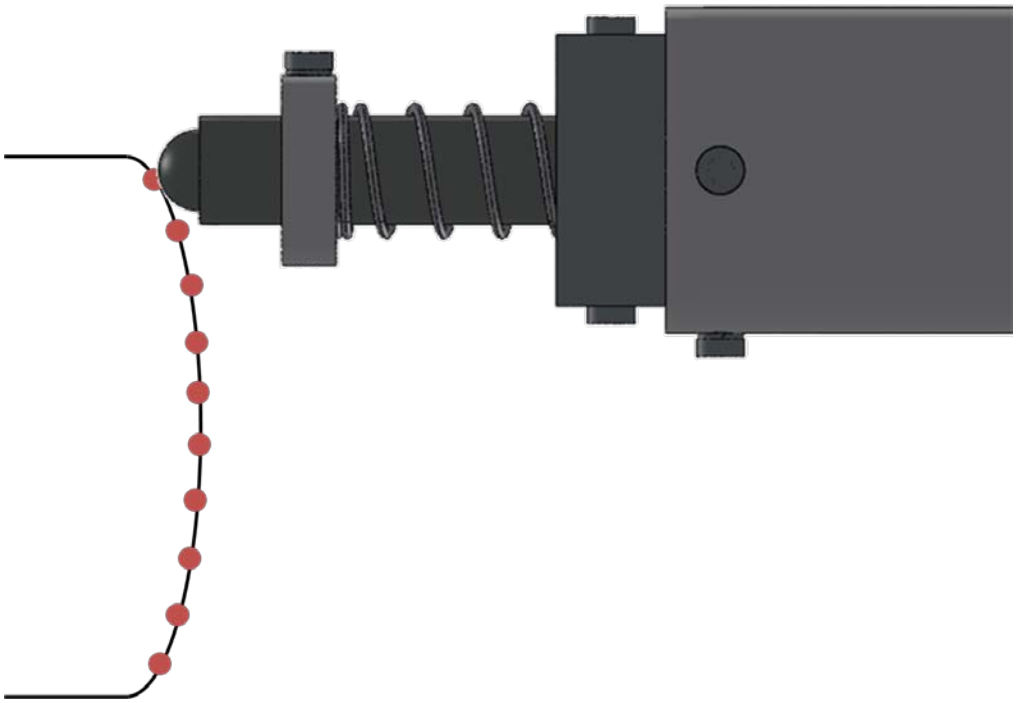

Figure 4-8. Bulge peak setup.

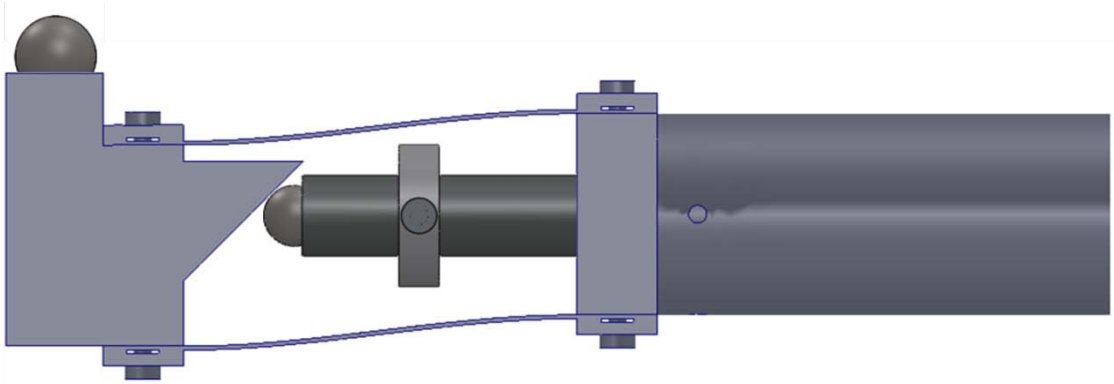

Figure 4-9. Flexure deflection.

# CHAPTER 5
# DATA ANALYSIS

In this chapter the conversion from LVDT voltage to displacement is discussed in detail for both measurement probes. The procedure for determining part dimensions from the displacement data is also presented.

## MATLAB Algorithm

As previously stated, the voltage data is post-processed using the MATLAB program included in Appendix B. A typical measurement result is saved (from LabVIEW) in one file that contains two columns, time and voltage, and all constants for the given measurement in separate columns. The MATLAB program reads in time and voltage as vectors and all constants as variables. The voltage vector is filtered using a Butterworth low pass filter with a cutoff frequency of 5 Hz. Figure 5-1 shows both the original and filtered data for a typical concentricity measurement. The time lag (phase shift) is a result of the filtering and, since it is constant, is ignored in the analysis.

Spindle encoder data was not accessible for synchronizing the beginning of spindle rotation to data acquisition. Therefore, an undetermined amount of random noise exists in the beginning of the voltage and time vector. A moving average calculation is used to determine the time at which the spindle rotation begins and the time and voltage vectors are truncated appropriately; see Figure 5-2. The unfiltered signal was used with this algorithm because it produced more accurate and consistent results.

The next step in the algorithm is to isolate one complete revolution of data. The reference point for identifying a single rotation was chosen to be the maximum value for the first Z-axis measurement. This point is then held constant for all additional

measurements of that workpiece in order to measure the change in offset as a function of hole depth. In order to find one complete cycle, a reference group of data points at the reference location is compared with subsequent groups of data. See Figure 5-3. Each group consists of 100 data points. Data is collected at 5000 Hz for 15 seconds for a total of 75000 points. Each subsequent group is spaced by one data point as shown in Figure 5-4. The difference between the reference group and each subsequent group is calculated and the group with the lowest difference is identified as the end location. The time between the reference point and the end location is used to transform the time axis into rotational angle. Figure 5-5 demonstrates the result. Calculations can now be performed according to Equation 5-2 in the following sections in order to obtain Figure 5-6.

**Length Probe Analysis**

As previously discussed in Chapter 4, reference values for the machine Z value ($Z_{ref}$) and voltage ($V_{ref}$) are obtained at the backstop and the measured voltage ($V_{meas}$) and new machine Z and X values ($Z_{loc}$ and $X_{peak}$ ) are obtained from actual workpiece measurements. The time-dependent measured voltage $V_{meas}$ is obtained from the face of the workpiece during rotation. Figure 5-7 shows length probe data that is output from the LVDT. The sinusoidal nature of the data suggests that the bulge protrusion on the face of the workpiece is not constant, but varies with angle. The cyclic nature of the data is present because data was collected for numerous rotations. Using the algorithm discussed in the preceding section, a single rotation is isolated and filtered for analysis. The conversion of voltage into length is performed using Equation 5-1. The result is shown in Figure 5-8.

$$L = (Z_{loc} - Z_{ref}) - \left(\frac{V_{meas} - V_{ref}}{K_L}\right) \quad (5\text{-}1)$$

- $Z_{loc}$ is the machine Z value when measuring the workpiece
- $Z_{ref}$ is the machine Z value when the reference voltage, $V_{ref}$, is calculated
- $V_{ref}$ is the voltage calculated when calibrating at the backstop
- $V_{meas}$ is the voltage measured during rotation of the workpiece
- $K_L$ is the calibration constant (0.64906 V/mm)

The two terms in Equation 5-1 each represent a distance that is required to calculate the total part length. Figure 5-9 demonstrates the physical meaning of these terms. The difference between $Z_{loc}$ and $Z_{ref}$ is the physical distance between the location of the turret (or a fixed spot on the probe) when it is measuring a part and its location when it is measuring the backstop. The second term represents the change in LVDT extension ($L_2$-$L_1$ in Figure 5-9) between the workpiece and backstop measurements. Together they yield the workpiece's total length.

### Concentricity Probe Analysis

The LVDT voltage that is recorded from the concentricity probe as the workpiece rotates provides information about both the radius of the hole and its offset from the center of the spindle axis (assumed to coincide with the workpiece outer diameter's axis of rotation). Figure 5-10 shows an exaggerated representation of the measurement as the workpiece rotates counterclockwise. The outer circle represents the workpiece outer diameter. The smaller solid circle represents the off-center hole. As the workpiece rotates, the center of the hole traces an even smaller circle represented by the dotted circle. The center offset of the hole, *o*, is the distance from the spindle axis to the center of the hole. The radius of the hole, *r*, is the perpendicular distance from the center of the hole to the surface of the inner diameter. The probe measures displacement along the x

direction only. Figure 5-11 and Equation 5-2 show how this relates to radius and center offset.

$$x = o\cos\theta + r\cos\varphi = o\cos\theta + r\cos\left(\sin^{-1}\left(\frac{o\sin\theta}{r}\right)\right) \quad (5\text{-}2)$$

Figure 5-6 shows the filtered output, x, of the sensor as a function of angle of rotation for a single rotation. The output, *x*, is the variation of the inner diameter surface location measured by the probe as the workpiece rotates. Due to the hole offset, the surface location is sinusoidal in nature. This output is calculated from the voltage using Equation 5-3.

$$x = \frac{(\mathrm{X_{loc}} - \mathrm{X_{ref}})}{2} + \left(\frac{V_{\mathrm{meas}} - \mathrm{V_{ref}}}{\mathrm{K_c}}\right) + r_{\mathrm{a}} \quad (5\text{-}3)$$

- $X_{loc}$ is the machine X value when measuring the workpiece
- $X_{ref}$ is the machine X value when the reference voltage, $V_{ref}$, is calculated
- $V_{meas}$ is the voltage measured during rotation of the workpiece
- $V_{ref}$ is the voltage calculated when calibrating with the artifact at $X_{ref}$
- $r_a$ is the radius of the calibration artifact
- $K_C$ is the calibration constant (0.62649 V/mm)

This equation is very similar to Equation 5-1 used for calculating part length. However, the term $r_a$ is required in Equation 5-3 because the reference voltage was not taken at a zero part reference location, but instead at a distance $r_a$ away from the spindle axis of rotation. Additionally, the sign change is necessary because an increase in diameter causes an increase in voltage, while an increase in part length corresponds to a decrease in voltage for Equation 5-1.

The data shown in Figure 5-6 can be used to calculate both the radius and center offset of the hole from the spindle axis at the selected Z-axis location. The radius is simply the midrange of the plot and the offset is the difference between the maximum and minimum values divided by two. The hole center location is determined by

comparing the results from different Z-axis locations. See Figure 5-12. The change in angle of the maximum value of the probe output can be used in conjunction with Equation 5-4 and Equation 5-5 to determine the x and y location of the offset.

$$x_c = o\cos(\Delta\theta) \tag{5-4}$$

$$y_c = o\sin(\Delta\theta) \tag{5-5}$$

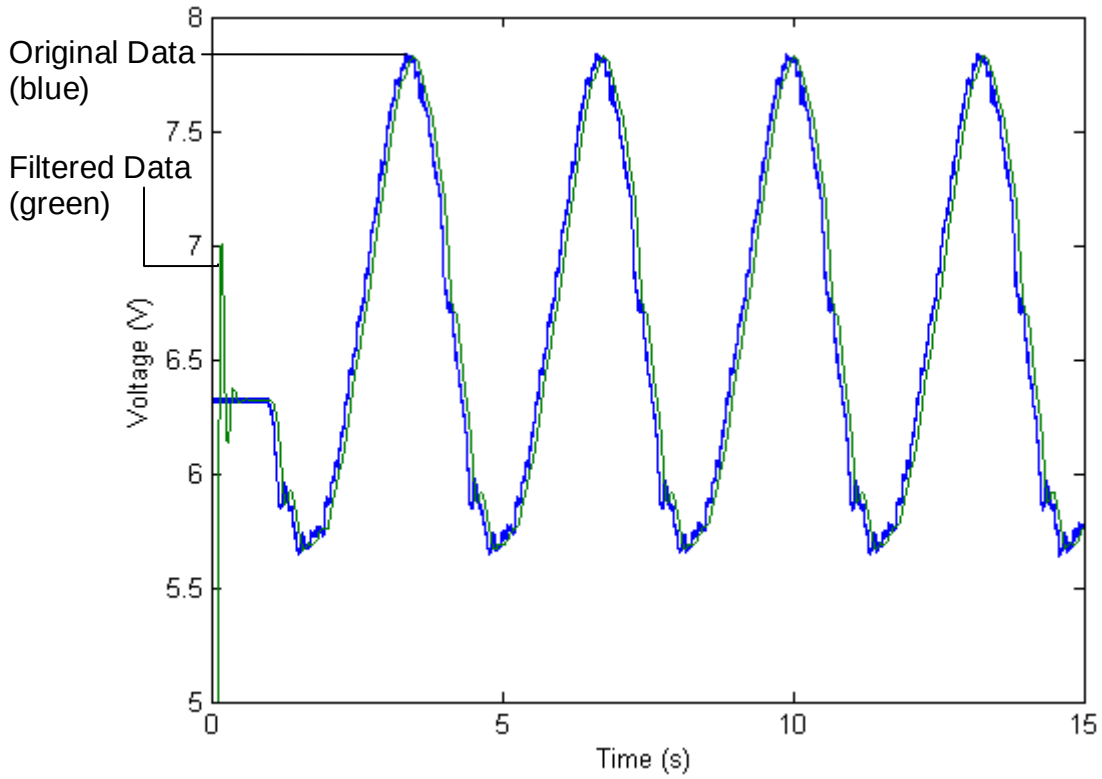


Figure 5-1. Original and filtered data.

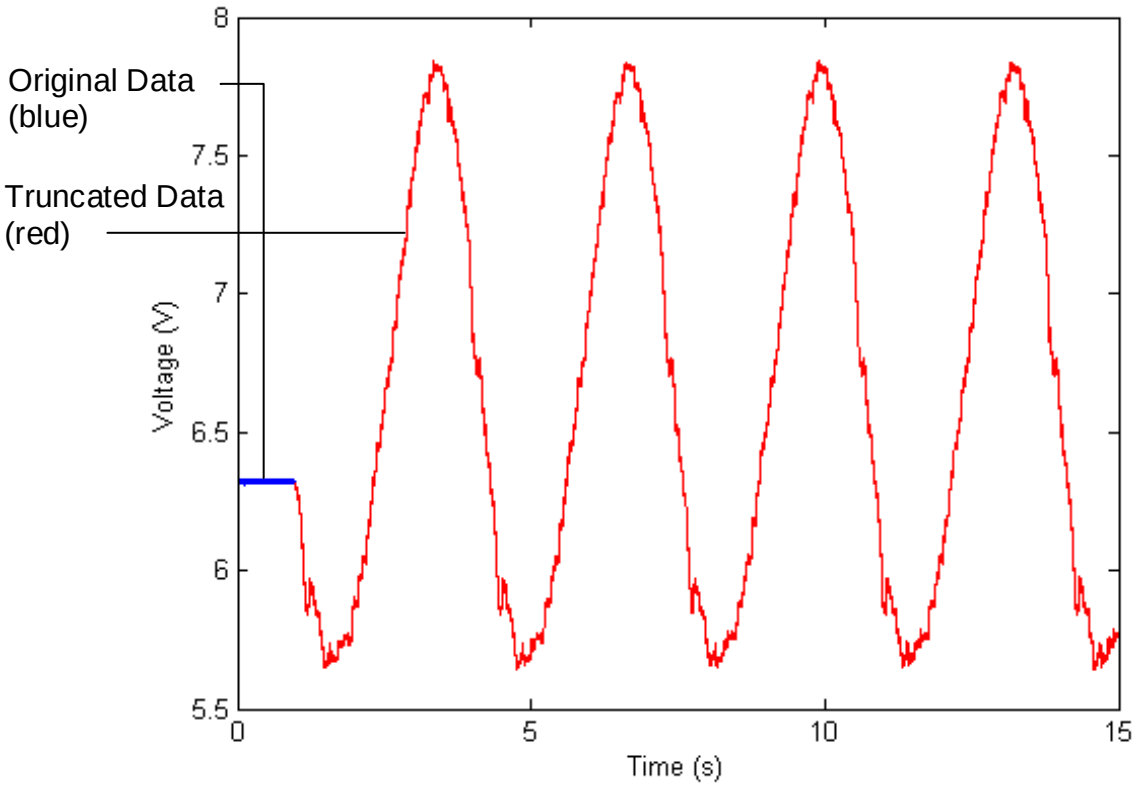


Figure 5-2. Time of initial data collection.

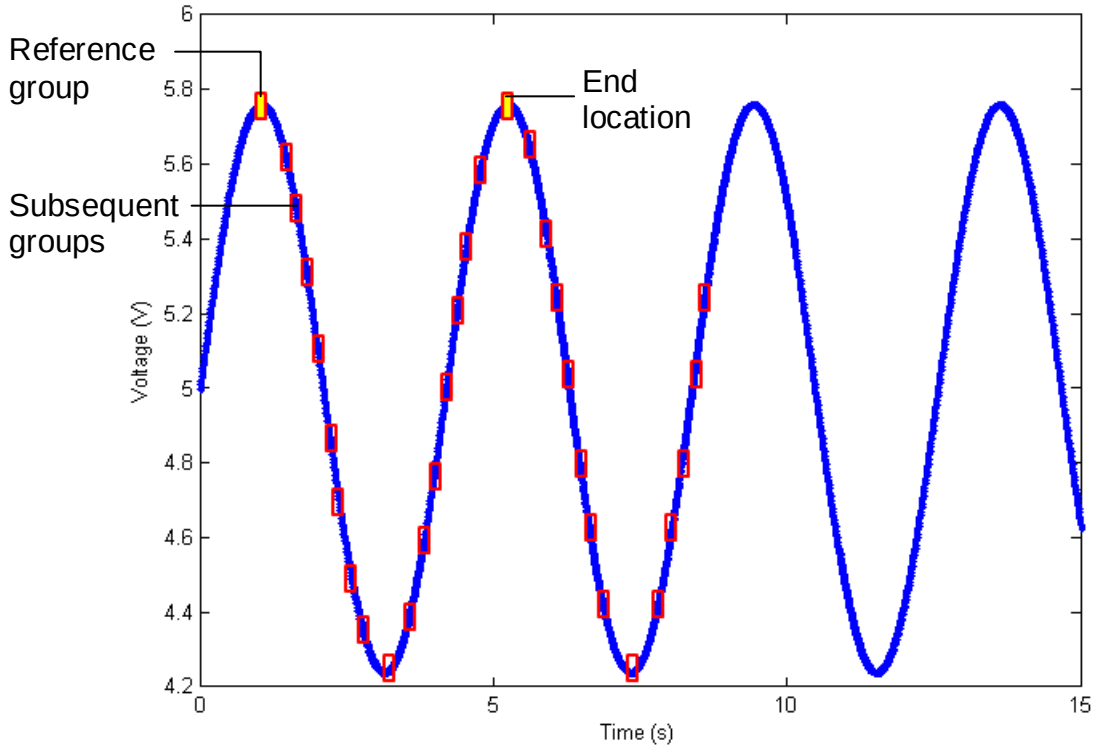


Figure 5-3. Data groups for isolating one rotation.

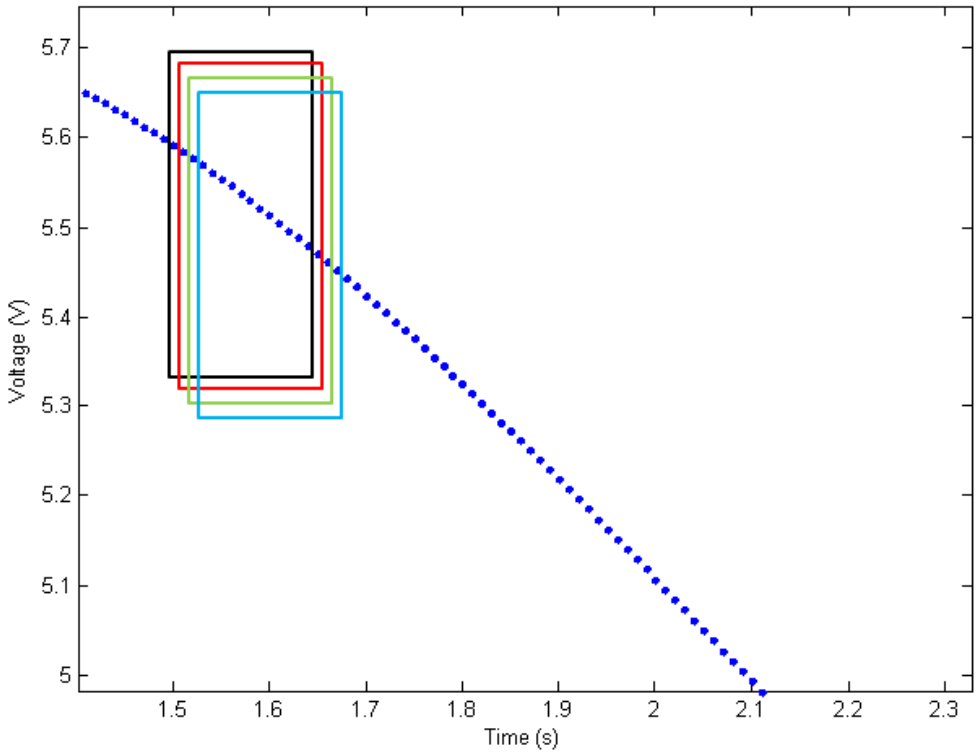


Figure 5-4. Spacing between subsequent groups.

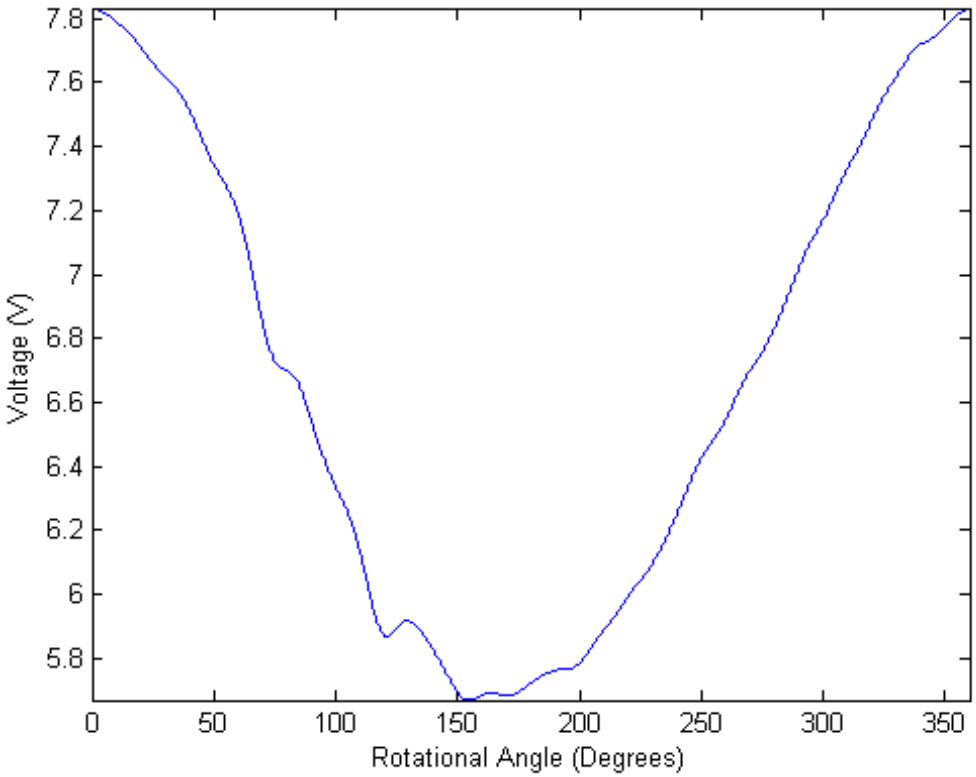


Figure 5-5. Single revolution of data.

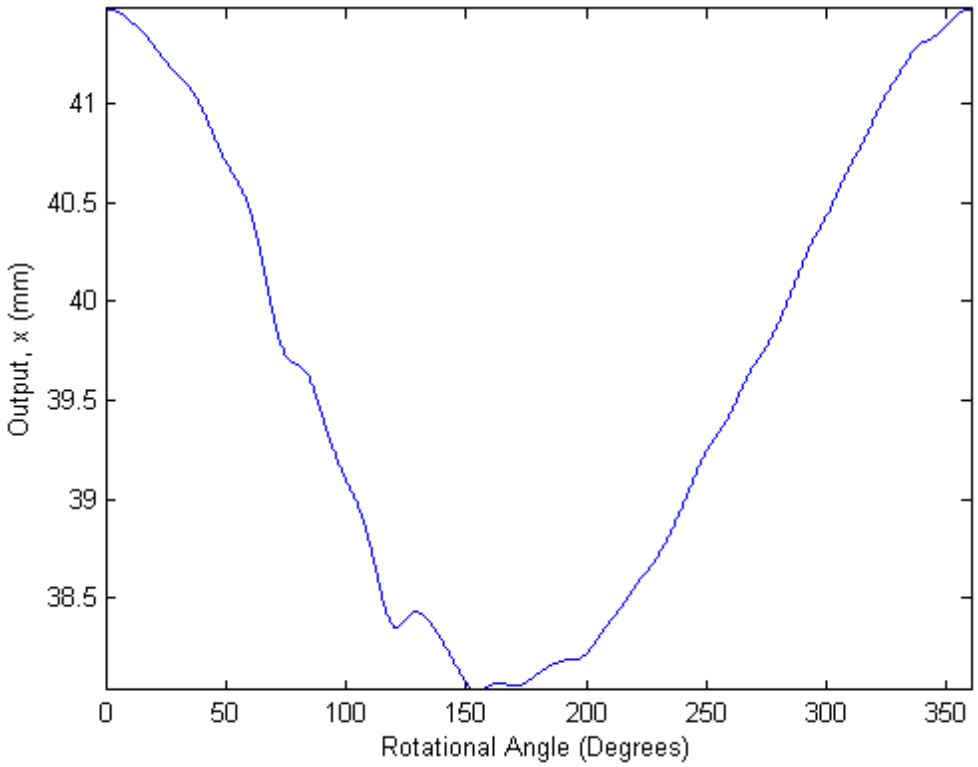


Figure 5-6. Concentricity data output.

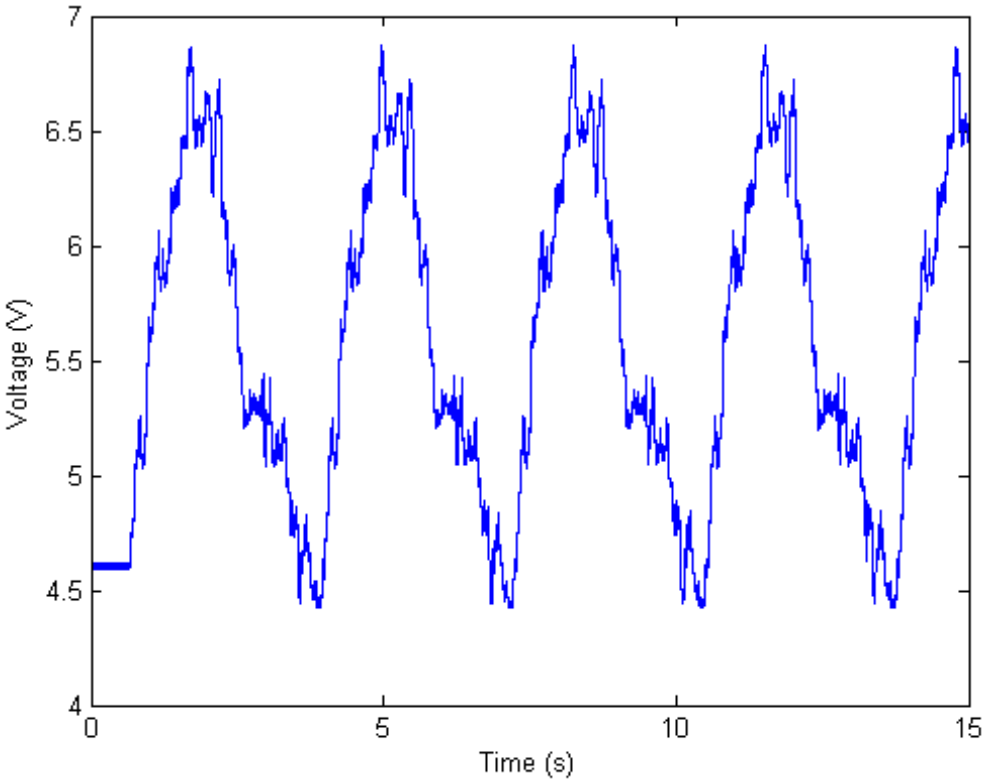


Figure 5-7. LVDT voltage data from the length probe.

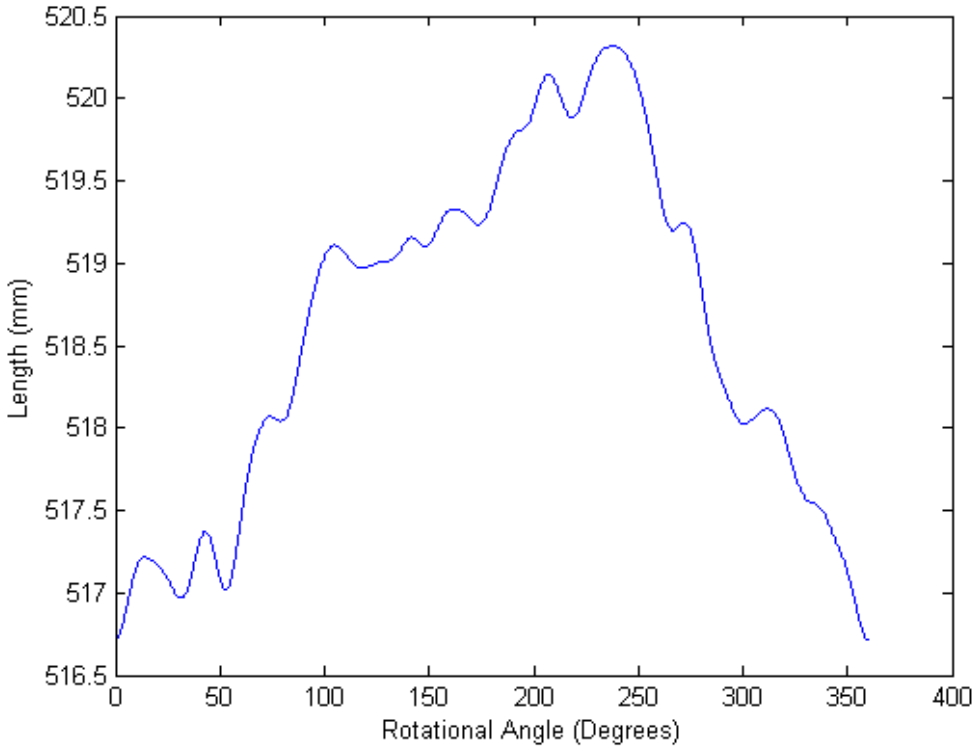


Figure 5-8. Final plot of length data.

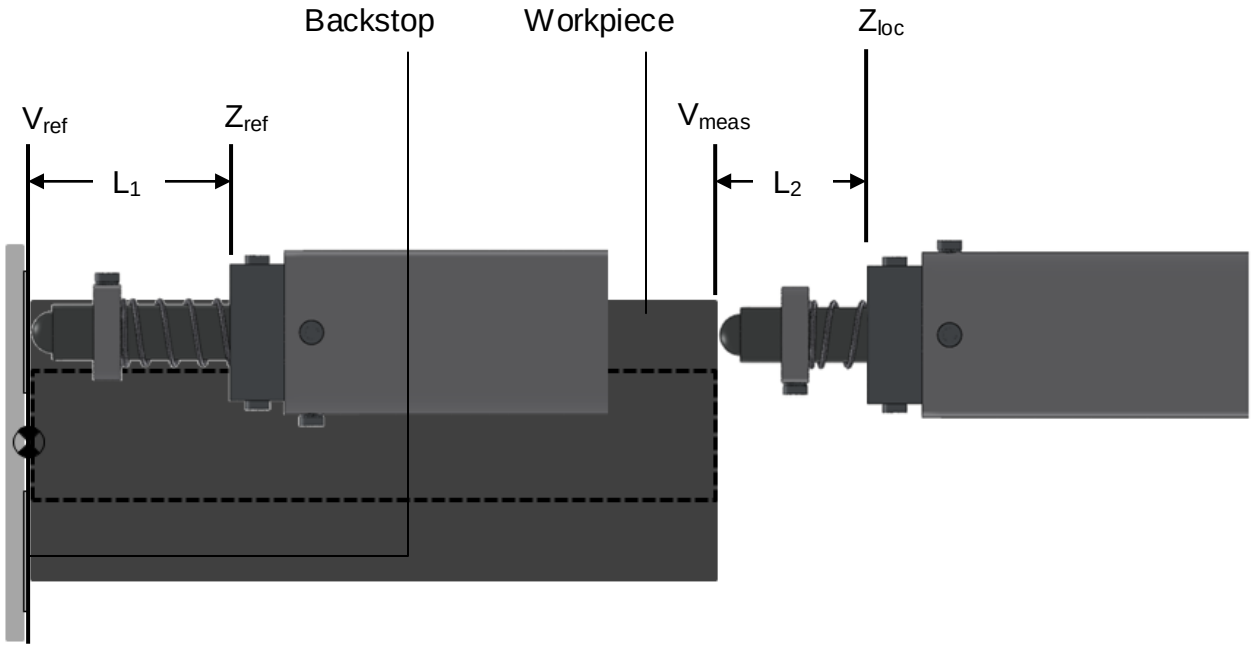


Figure 5-9. Workpiece measurements.

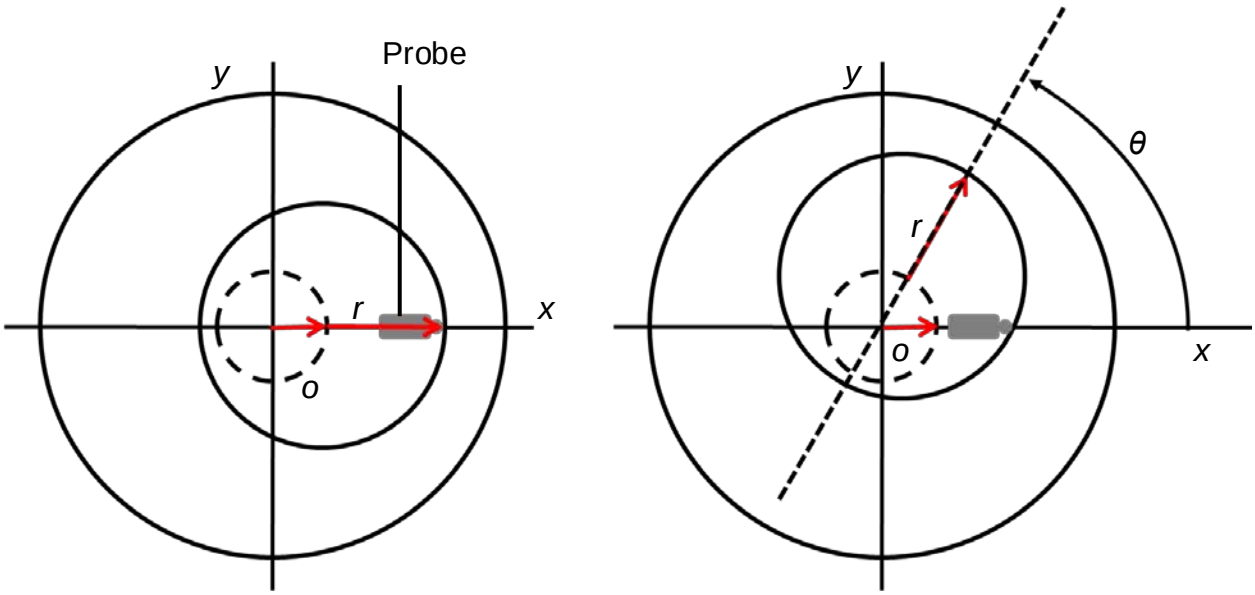


Figure 5-10. Concentricity measurement.

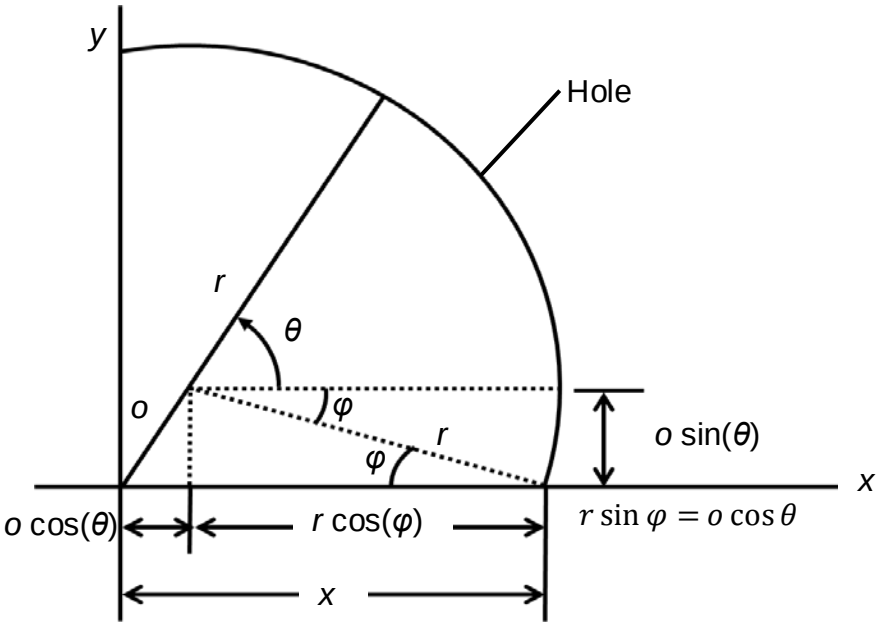


Figure 5-11. Relationship between measurement and radius and offset.

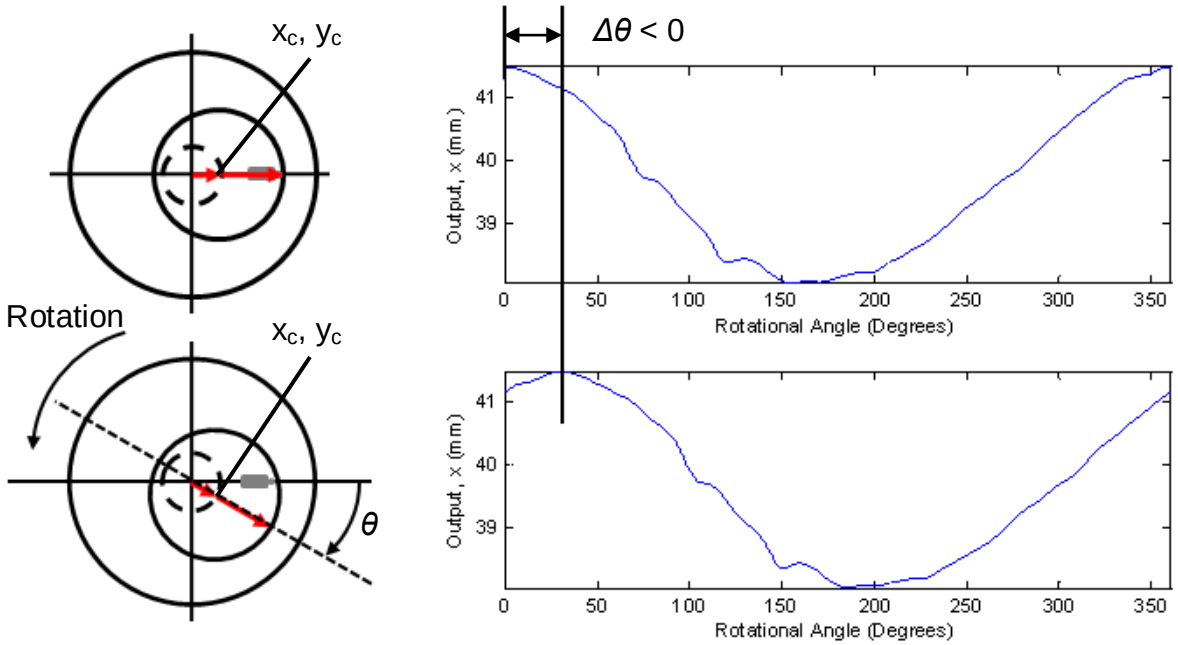


Figure 5-12. Data for different Z-axis locations.

# CHAPTER 6
# RESULTS AND DISCUSSION

## Length Results

The tool joint dimensions in Figure 1-4 indicate a part length of 520.7 mm with a tolerance of -0/+6.35 mm. A total of 12 workpieces were measured; see Figure 6-1. The length measurements are provided in Table 6-1. The values correlate well with the dimensions specified for the forged workpiece. Only two parts (parts 2 and 8 bolded in Table 6-1) were out of tolerance. The location of the bulge on the face of the part (see Figure 4-8) was also consistent, typically occurring 116 mm from the spindle axis, with the exception of part 6.

Additional measurements were conducted on a separate occasion (requiring rechucking of the workpiece) in order to check for consistency. The entire setup was repeated, including a recalibration of the probe. Part 11 was measured 4 additional times without rechucking in between measurements. The resulting lengths were found to be {521.272, 521.269, 521.266, 521.266, and 521.264 mm}. Although the range is only 0.008 mm (0.001%), the first value differs from the previous setup's value of 521.035 mm by 0.237 mm (0.04%). Part 1 was also rechucked and measured and its value differed by 0.216 mm (0.04%). This difference is believed to be attributed to inconsistency in chucking. The difference between measured length and true length is shown in Figure 6-2. Each time a workpiece is chucked, there is potential for a $\Delta L$ change in length of the workpiece. A dial indicator was used to measure runout of the outer diameter at the tip of the workpiece. Typical values of lateral runout ranged from ±0.61mm to ±2.2 mm. This can produce length measurements that deviate by 0.181

mm to 0.680 mm from nominal. Figure 6-3 and Equations 6-1 to 6-6 show how this value is determined.

$$\Delta L = L_{\text{meas}} - L_{\text{true}} \tag{6-1}$$

$$L_{\text{true}} = \sqrt{r^2 + {x_1}^2} \tag{6-2}$$

$$x_1 + x_2 = L_{\text{meas}} \tag{6-3}$$

$$\tan\theta = \frac{r}{x_1} \tag{6-4}$$

$$\sin\theta = \frac{x_2}{W} \tag{6-5}$$

$$W = W_2 + \frac{W_1 - W_2}{2} \tag{6-6}$$

- $L_{\text{meas}}$ is the length obtained from the LVDT probe
- $L_{\text{true}}$ is the actual workpiece length that is unknown
- $r$ is the measured radial runout
- $W_1$ is the larger outside diameter of the workpiece
- $W_2$ is the smaller outside diameter of the workpiece
- $x_1$, $x_2$, $\theta$, and $W$ are geometrical variables in Figure 6-3

Table 6-1. Length measurements results (values out of tolerance are in bold).

| Part # | Bulge location (mm from center) | Length (mm) |
|---|---|---|
| 1 | 128.016 | 521.609 |
| 2 | 102.870 | **520.316** |
| 3 | 113.538 | 521.800 |
| 4 | 106.680 | 521.068 |
| 5 | 128.270 | 523.743 |
| 6 | 99.314 | 523.921 |
| 7 | 121.920 | 521.528 |
| 8 | 121.158 | **520.639** |
| 9 | 121.920 | 523.029 |
| 10 | 123.190 | 522.930 |
| 11 | 111.760 | 521.035 |
| 12 | 114.300 | 523.464 |
| Mean | 116.078 | 522.090 |
| Range | 28.956 | 3.604 |

## Concentricity Results

The tool joint dimensions given in Figure 1-4 indicate a hole radius of 40.767 mm with a tolerance of +0/-0.635 mm. Table 6-2 provides the results for measurements taken with the concentricity probe. Measurements were taken at {6.35, 63.5, 127, and 190.5} mm from the front of the workpiece. Some measurements deviated from these locations in order to avoid deep pits or chunks of metal that protruded from the surface of the hole that would skew results and potentially damage the sensor. Only three radius measurements were within the tolerance specified. All other values were smaller by an average of 0.271 mm.

A substantial amount of debris was present on the contact sphere after each measurement. See Figure 6-4. Although the contact sphere was cleaned and lubricated prior to each measurement, debris that collected during measurement is believed to have biased the result to a smaller value. The problem is believed to be attributed to the fact that the available workpieces had been exposed to harsh outside conditions prior to being shipped for study. This produced worse than average surface rust, which was difficult to remove uniformly (the surface was cleaned with steel brush).

Similar to the length probe measurements, additional concentricity measurements were conducted in order to check for consistency with and without rechucking. Part 11 was measured 5 additional times at each depth without rechucking in between measurements. The results are shown in Table 6-3. Center offset and location measurements for values taken without rechucking ranged by an average of 0.001 mm and 0.015 mm respectively. Radius varied by an average of 0.003 mm (0.006% change). With rechucking however, the data varied greatly. Only the radius

measurement exhibited consistency from a previous clamped workpiece, varying by an average of 0.069 mm (0.17% change). Again, this suggests chucking inconsistency.

Table 6-2. Concentricity measurements results (values out of tolerance are in bold).

| Part # | Distance from front (mm) | Center offset (mm) | Radius (mm) | $x_c$ (mm) | $y_c$ (mm) |
|---|---|---|---|---|---|
| 1 | 6.35 | 1.317 | **39.812** | 1.317 | 0.000 |
| | 63.5 | 0.917 | 40.218 | 0.908 | -0.125 |
| | 127 | 0.878 | **39.870** | 0.793 | -0.375 |
| | 190.5 | 0.965 | **39.863** | 0.864 | -0.430 |
| 2 | 6.35 | 1.306 | **39.858** | 1.306 | 0.000 |
| | 82.55 | 0.474 | **39.949** | 0.335 | 0.335 |
| | 95.377 | 0.497 | **39.787** | 0.201 | 0.455 |
| | 184.15 | 0.471 | **39.517** | -0.471 | 0.016 |
| 3 | 6.35 | 1.337 | **39.837** | 1.337 | 0.000 |
| | 63.5 | 0.923 | 40.069 | 0.918 | 0.095 |
| | 127 | 0.766 | **39.832** | 0.694 | -0.322 |
| | 190.5 | 0.706 | **39.835** | 0.489 | -0.509 |
| 4 | 6.35 | 1.439 | **40.063** | 1.439 | 0.000 |
| | 63.5 | 1.381 | 40.132 | 1.152 | -0.762 |
| | 127 | 1.341 | **39.776** | 1.309 | -0.291 |
| | 190.5 | 1.373 | **39.870** | 1.360 | 0.190 |
| 5 | 6.35 | 2.751 | **39.815** | 2.751 | 0.000 |
| | 63.5 | 2.301 | **40.063** | 2.300 | 0.060 |
| | 127 | 1.947 | **39.710** | 1.947 | 0.004 |
| | 214.35 | 1.721 | **39.756** | 1.714 | -0.148 |
| 6 | 6.35 | 1.904 | **39.743** | 1.904 | 0.000 |
| | 63.5 | 1.588 | **40.071** | 1.587 | -0.045 |
| | 127 | 1.350 | **39.921** | 1.305 | -0.344 |
| | 190.5 | 1.130 | **39.868** | 1.074 | -0.351 |
| 7 | 6.35 | 1.467 | **39.901** | 1.467 | 0.000 |
| | 63.5 | 1.474 | **40.107** | 1.474 | -0.039 |
| | 127 | 1.372 | **39.817** | 1.365 | -0.135 |
| | 190.5 | 1.350 | **39.837** | 1.325 | 0.258 |
| 8 | 6.35 | 2.286 | **39.995** | 2.286 | 0.000 |
| | 63.5 | 1.441 | **40.013** | 1.385 | -0.396 |
| | 127 | 1.012 | **39.812** | 0.957 | -0.329 |
| | 162.09 | 0.776 | **39.748** | 0.741 | -0.231 |
| 9 | 6.35 | 1.913 | **40.056** | 1.913 | 0.000 |
| | 63.5 | 0.789 | **40.119** | 0.696 | 0.372 |

Table 6-2. Continued

| Part # | Distance from front (mm) | Center offset (mm) | Radius (mm) | $x_c$ (mm) | $y_c$ (mm) |
|---|---|---|---|---|---|
| | 127 | 0.234 | **39.715** | 0.220 | 0.078 |
| | 190.5 | 0.548 | **39.766** | -0.546 | 0.049 |
| 10 | 6.35 | 1.359 | **39.756** | 1.359 | 0.000 |
| | 63.5 | 0.911 | **39.926** | 0.798 | 0.439 |
| | 127 | 0.946 | **39.505** | 0.873 | 0.363 |
| | 190.5 | 0.643 | **39.517** | 0.582 | 0.274 |
| 11 | 6.35 | 0.920 | **39.705** | 0.920 | 0.000 |
| | 63.5 | 0.717 | **40.063** | 0.604 | 0.386 |
| | 127 | 0.640 | **39.726** | 0.637 | 0.058 |
| | 190.5 | 0.596 | **39.530** | 0.590 | -0.089 |
| 12 | 6.35 | 1.571 | **40.094** | 1.571 | 0.000 |
| | 63.5 | 0.882 | **40.107** | 0.847 | -0.248 |
| | 127 | 0.735 | **39.647** | 0.429 | -0.597 |
| | 190.5 | 0.591 | **39.632** | -0.272 | -0.525 |
| Mean | | 1.166 | 39.861 | 1.057 | -0.060 |
| Range | | 2.517 | 0.714 | 3.297 | 1.217 |

Table 6-3. Concentricity repeatability results without rechucking.

| Distance from front (mm) | Measurement number | Center offset (mm) | Radius (mm) | $x_c$ (mm) | $y_c$ (mm) |
|---|---|---|---|---|---|
| | 1 | 0.175 | 39.825 | 0.175 | 0.000 |
| | 2 | 0.176 | 39.825 | 0.176 | -0.002 |
| 6.35 | 3 | 0.177 | 39.827 | 0.177 | -0.004 |
| | 4 | 0.177 | 39.827 | 0.177 | -0.002 |
| | 5 | 0.177 | 39.827 | 0.177 | -0.006 |
| | Mean | 0.176 | 39.826 | 0.176 | -0.003 |
| | Range | 0.002 | 0.003 | 0.002 | 0.006 |
| | 1 | 0.289 | 40.114 | 0.289 | 0.000 |
| | 2 | 0.289 | 40.114 | 0.289 | 0.000 |
| 63.5 | 3 | 0.290 | 40.114 | 0.290 | 0.006 |
| | 4 | 0.290 | 40.117 | 0.290 | 0.000 |
| | 5 | 0.291 | 40.117 | 0.291 | 0.014 |

Table 6-3. Continued

| Distance from front (mm) | Measurement number | Center offset (mm) | Radius (mm) | $x_c$ (mm) | $y_c$ (mm) |
|---|---|---|---|---|---|
| | Mean | 0.290 | 40.115 | 0.290 | 0.004 |
| | Range | 0.001 | 0.003 | 0.001 | 0.014 |
| 127 | 1 | 0.286 | 39.731 | 0.286 | 0.000 |
| | 2 | 0.286 | 39.733 | 0.286 | 0.012 |
| | 3 | 0.287 | 39.733 | 0.286 | -0.021 |
| | 4 | 0.287 | 39.736 | 0.286 | -0.020 |
| | 5 | 0.287 | 39.736 | 0.287 | -0.019 |
| | Mean | 0.287 | 39.734 | 0.286 | -0.010 |
| | Range | 0.002 | 0.005 | 0.001 | 0.034 |
| 190.5 | 1 | 0.324 | 39.627 | 0.324 | 0.000 |
| | 2 | 0.323 | 39.627 | 0.323 | -0.005 |
| | 3 | 0.324 | 39.627 | 0.324 | -0.007 |
| | 4 | 0.324 | 39.627 | 0.324 | 0.000 |
| | 5 | 0.324 | 39.627 | 0.324 | -0.005 |
| | Mean | 0.324 | 39.627 | 0.324 | -0.004 |
| | Range | 0.000 | 0.000 | 0.000 | 0.007 |
| | Average Range | 0.001 | 0.003 | 0.001 | 0.015 |

## Verification of Probe Accuracy

As stated in Chapter 4, an artifact was used to verify the probe's performance. Measurements of the artifact with the probes are compared to dimensions obtained using CMM in Table 6-4. The probes' values show good agreement with CMM results. LVDT probe values were slightly greater than that measured with the CMM.

The probe's average length measurement was 0.022 mm larger than the CMM measurement or a 0.007% difference. As explained previously, this can be due to imperfect chucking as seen in Figure 6-2. Radius measurement of the artifact also produced results larger than those measured with CMM by 0.041 mm or 0.053%

change. Considering the fact that a fixed calibration constant was used to account for misalignment in the device, sensor noise causes an uncertainty of ±0.038 mm, and the CMM has an uncertainty of 0.012 mm over its work volume; this result is considered acceptable. Center offset was significantly different however, varying by over 50%. Since the artifact is not perfectly round, the CMM fits a circle to the probed data points; while the LVDT probe simply uses the difference between maximum and minimum displacements to calculate offset. This could potentially shift the center of the circle in the direction of noncircular areas for the LVDT. See Figure 6-5. Additionally, since an encoder was not available to start recording data at the same time as the spindle began its rotation (the MATLAB algorithm was used to select the location instead), there is a level of uncertainty associated with the location of maximum radius, which alters the values for center location substantially.

Table 6-4. Artifact verification.

| Measurement | CMM | Probe | Difference |
|---|---|---|---|
| Length (mm) | 316.662 | 316.684 | -0.022 |
| Radius (mm) | 77.221 | 77.262 | -0.041 |
| Center Offset (mm) | 0.014 | 0.006 | 0.008 |

Figure 6-1. Measured workpieces.

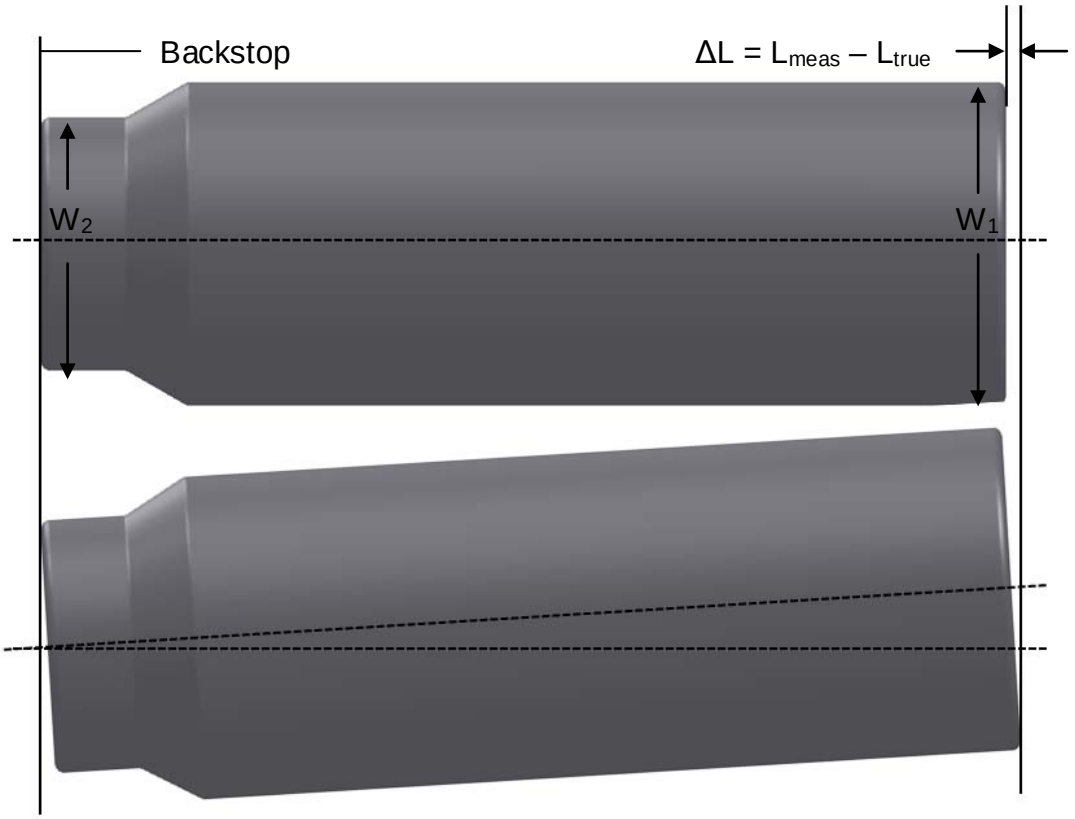


Figure 6-2. Workpiece length variation due to imperfect chucking.

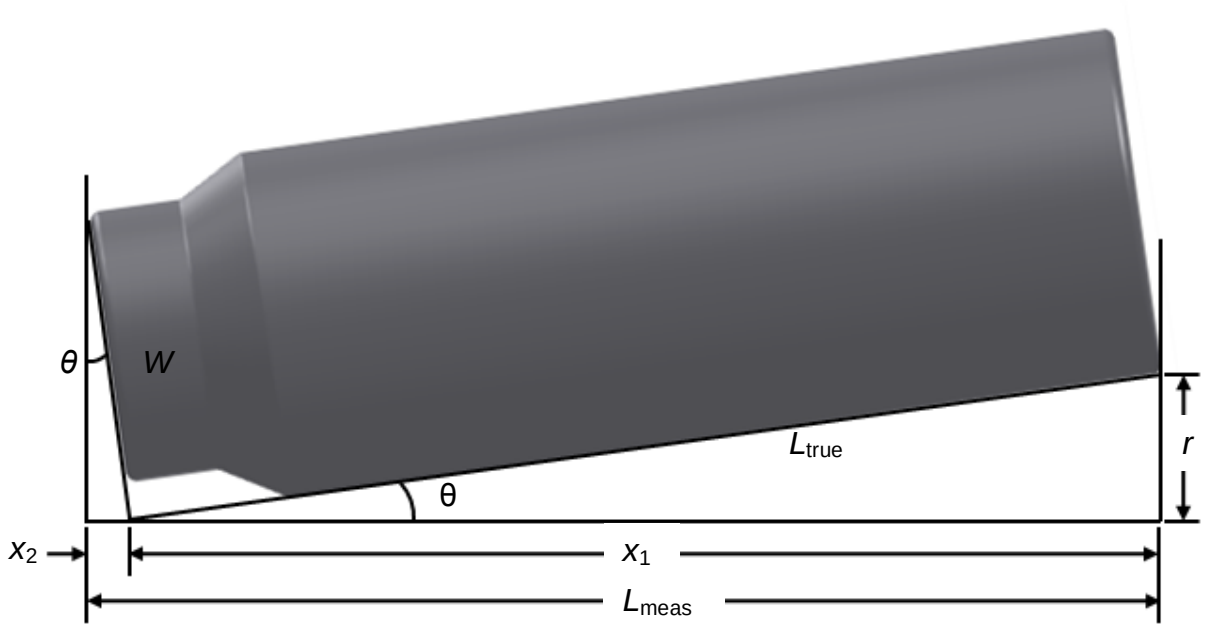


Figure 6-3. Explanation of length variation.

Figure 6-4. Condition of contact sphere after measurement.

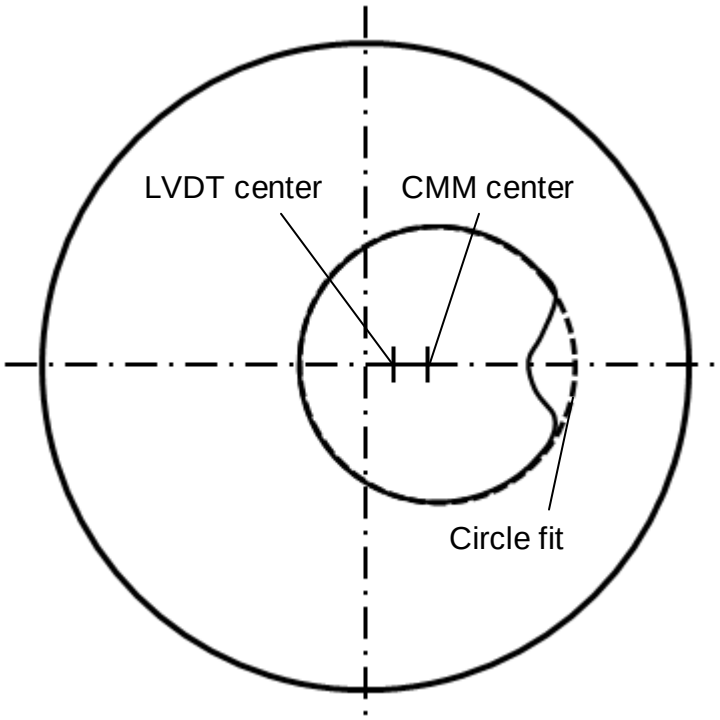

Figure 6-5. Offset shift due to non circular part.

# CHAPTER 7
# CONCLUSIONS

In this study, a solution to a conservative and time-consuming machining strategy in order to account for geometrical variations of forgings was presented. Two LVDT-based contact probes were designed and implemented for measuring workpiece length and concentricity prior to machining. The length measuring probe consists of an LVDT that is spring loaded against a shaft which contacts the workpiece via a hardened stainless steel precision ball. The concentricity probe also uses an LVDT and shaft, but includes a parallelogram leaf-type flexure and 45° platform to transfer motion from the machine x-axis to the LVDT and machine z-axis.

The devices were used to measure 12 forged tool joints. After thorough testing, both devices proved to be acceptably accurate. The length probe displayed a repeatability of 8 µm, whereas the concentricity probe had a repeatability of 3 µm. Using an artifact of known dimensions, the probes measured length and radius to within 0.007% and 0.053% of CMM results. It is important to note that the goal of the contact probes were not to measure the actual dimensions of the workpiece, but to identify where the tool will make initial contact with the workpiece surface. Therefore, differences in dimensions between the artifact when it is chucked in the machine or measured on the CMM is not necessarily a problem for this application.

Overall, the LVDT probes were successful in measuring workpiece dimensions and proved to be robust and sufficiently accurate for consideration in industrial application. A potential course of action would be to use the measured dimensions to select from a list of part programs that are designed for a range of part dimensions. See Table 7.1.

Future work should focus on synchronizing the angular displacement of the workpiece to the data acquisition. Additionally, alignment errors associated with the assembly of the concentricity probe should be improved. Design changes to remove hysteresis from the concentricity probe would also increase the device's accuracy. Inconsistencies in the chucking process should also be explored.

After a redesign of the probes, a more efficient measurement procedure should be established for industrial application in order to minimize non-cutting time. Rather than completing measurements at discrete depths and locations, a continuous measurement could easily be implemented to obtain a more accurate and complete description of the workpiece in a shorter amount of time. Calculations should be performed at the conclusion of measurement via LabVIEW instead of post-processed with MATLAB so that automatic and instantaneous part program changes based on measurement results can be implemented instead of having to choose between programs. This would require an additional device to record the machine position during measurement. Lastly, a cost-benefit analysis should be conducted to determine the advantage of implementing this solution versus a redesign of the forging process.

Table 7-1. Selection of part programs to cover ranges in workpiece geometric variations.

| Length/Diameter | **Small** | **Medium** | **Large** |
|---|---|---|---|
| **Small** | Part program1 | 4 | 7 |
| **Medium** | 2 | 5 | 8 |
| **Large** | 3 | 6 | 9 |

APPENDIX A
LABVIEW PROGRAM

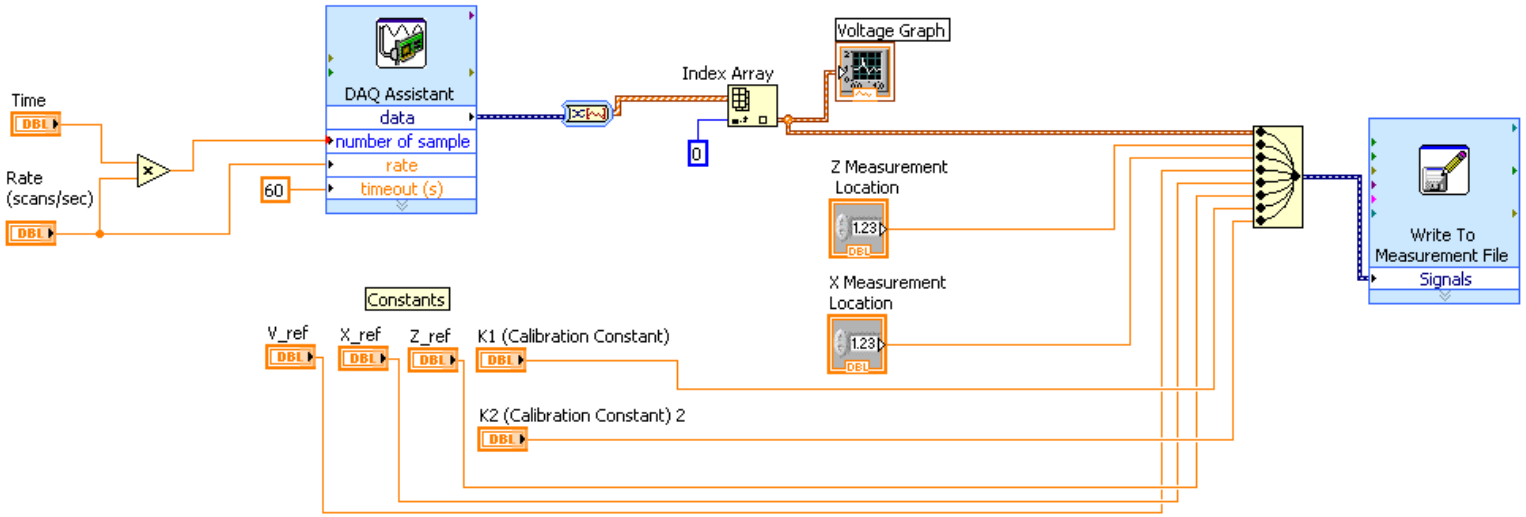


Figure A-1. LabVIEW block diagram.

# APPENDIX B
# MATLAB PROGRAM

```
% Arthur Graziano
% 01/23/10

clear all
close all
clc

%% READ DATA

% Concentricity
% z=xlsread('C:\Documents and
        Settings\graziano\Desktop\DATA\Part12\Concentricity\four.xlsx','A24:B75023');
% z_loc=xlsread('C:\Documents and
        Settings\graziano\Desktop\DATA\Part12\Concentricity\four.xlsx','C24:C25');
% x_loc = xlsread('C:\Documents and
        Settings\graziano\Desktop\DATA\Part12\Concentricity\four.xlsx','D24:D25');

% Length
% L=xlsread('C:\Documents and
        Settings\graziano\Desktop\DATA\Part12\Length\rotate.xlsx','A24:B75023');
% Z_peak = xlsread('C:\Documents and
        Settings\graziano\Desktop\DATA\Part12\Length\rotate.xlsx','D24:D25');
% X_peak = xlsread('C:\Documents and
        Settings\graziano\Desktop\DATA\Part12\Length\rotate.xlsx','C24:C25');

%% NOISE FILTERING

warning 'OFF'

% sampling freqency
fs=5e3;

% fft spectrum
[V1,f]=spec(zeropad(z(:,2),2^16),fs);

% low pass filter section
% cut-off frequency
fcut=5;

% butterworth low pass filter
[b,a]=butter(4,2*fcut/fs,'low');
Hhp=freqz(b,a,2*pi*f/fs);
vf1=filter(b,a,z(:,2));

figure
plot(z(:,1),[z(:,2), vf1])
title('Concentricity Data')

%%Length%%

[V2,f2]=spec(zeropad(L(:,2),2^16),fs);
```

```
Hhp2=freqz(b,a,2*pi*f2/fs);
vf2=filter(b,a,L(:,2));

figure
plot(L(:,1),[L(:,2),vf2])
title('Length Data')

%% INITIAL CONDITIONS

% Day 1
% V_ref = 8.6466957; %Most round data (median of cycle one)
% x_ref = 3.267;
% D_ref = 6.0010866;
% K = 15.913; %V/in
%
% Z_ref=-13.1698; %backstop
% V_ref2=3.9996927;
% L_ref=0;
% K2=16.486; %V/in

% Day 2

% Bottom Diameter (two)
V_ref = 7.514675;
x_ref = 3.4374;
D_ref = 152.9518/25.4;
K = 16.467;

Z_ref=-12.8853; %backstop
V_ref2=5.07002;
L_ref=0;
K2=16.265; %V/in

%% DATA START

%Finds at what time the part begins to rotate
sens = 0.00025;
stp = 100;
rot=zeros(30000-stp,1);

%Moving average calculation
rot(1,1)=z(1,2);
rot(2,1)=(rot(1,1)+z(2,2))/2;
for i = 3:30000-stp
    rot(i,1)=(z(i,2)+((i-1)*rot(i-1,1)))/(i);
end
for i=1000:length(rot)-stp
    rot(i,2)=rot(i+stp,1)-rot(i,1);
end


rot1=find(abs(rot(:,2))>sens);
t0=rot1(1)+0.5*stp;                %index where it begins to rotate

time0=(t0-1)/fs;          %time where it begins to rotate
```

```
figure
plot(z(:,1),z(:,2),'b',z(t0:end,1),z(t0:end,2),'r'); % Check data when rotating
title('Check if noise removal is appropriate (concentricity)')
xlabel('Time (s)')
ylabel('Voltage (V)')


% Deletes data before rotation and updates time vector
z1(:,1)=z(:,1);
z1(:,2)=vf1;
z1(1:t0,:)=[];
for i=1:length(z1)
    z1(i)=z1(i)-(time0+0.0002);
end

figure
plot(z1(:,1),z1(:,2))
title('Pick Start time for single rotation (Concentricity)')
xlabel('Time (s)')
ylabel('Voltage (V)')

%% Length%%

%Finds at what time the part begins to rotate
sens = 0.00025;
stp = 100;
rot2=zeros(30000-stp,1);

%Moving average calculation
rot2(1,1)=L(1,2);
rot2(2,1)=(rot2(1,1)+L(2,2))/2;
for i = 3:30000-stp
    rot2(i,1)=(L(i,2)+((i-1)*rot2(i-1,1)))/(i);
end
for i=1000:length(rot2)-stp
    rot2(i,2)=rot2(i+stp,1)-rot2(i,1);
end

rot1_2=find(abs(rot2(:,2))>sens);
t0_2=rot1_2(1)+0.5*stp;                %index where it begins to rotate

time0_2=(t0_2-1)/fs;          %time where it begins to rotate

% figure
% plot(L(:,1),L(:,2),'b',L(t0_2:end,1),L(t0_2:end,2),'r'); % Check data when rotating
% title('Check if noise removal is appropriate (Length)')
% xlabel('Time (s)')
% ylabel('Voltage (V)')

% Deletes data before rotation and updates time vector
L1(:,1)=L(:,1);
L1(:,2)=vf2;
L1(1:t0_2,:)=[];
for i=1:length(L1)
    L1(i)=L1(i)-(time0_2+0.0002);
end
```

```
figure
plot(L1(:,1),L1(:,2))
title('Pick Start time for single rotation (Length)')
xlabel('Time (s)')
ylabel('Voltage (V)')

%% FIND ONE COMPLETE CYCLE

r=fs;         % scan rate
time = input('Pick start time for concentricity (x.xxxx sec)'); % start point (keep constant for entire part)
% time = 3.6345;
t1=round(time*r + 1);

v1=(t1:t1+99)'; %initial indices (100) for comparison

a=length(z1);
b=length(v1);

% taking difference between initial indices and future indices
% Note: limited to 24,000 to avoid picking 2 cycles as one.

stp=500;
dif=cell(24000,2);
% dif=cell(a-t1-b-stp,2);
for i=1:24000 %a-t1-b-stp
   dif{i,1}=z1(round(v1),2)-z1(round(v1+stp+i),2);
end

% sums the total difference for the entire v1 vector for each dif
for j=1:length(dif)
dif{j,2}=sum(abs(dif{j,1}(:,1)));
end

% finds the location where there is a minimum difference between the v1
% vector
dif2=cell2mat(dif(:,2));
t2=find(dif2==min(dif2))+t1+stp;        % index at end of 1 cycle

time2=((t2-t1)/r)+time;                % time at end of 1 cycle

% Length%

% time_2 = input('Pick start time for length (x.xxxx sec)'); % start point (keep constant for entire part)
time_2 = 4.129;
t1_2=round(time_2*r + 1);

v1_2=(t1_2:t1_2+99)'; %initial indices (100) for comparison

a=length(L1);
b=length(v1_2);

% taking difference between initial indices and future indices
% Note: limited to 24,000 to avoid picking 2 cycles as one.

stp=500;
```

```
dif_2=cell(24000,2);
% dif=cell(a-t1-b-stp,2);
for i=1:24000 %a-t1-b-stp
   dif_2{i,1}=L1(round(v1_2),2)-L1(round(v1_2+stp+i),2);
end

% sums the total difference for the entire v1 vector for each dif
for j=1:length(dif_2)
dif_2{j,2}=sum(abs(dif_2{j,1}(:,1)));
end

% finds the location where there is a minimum difference between the v1
% vector
dif2_2=cell2mat(dif_2(:,2));
t2_2=find(dif2_2==min(dif2_2))+t1_2+stp;        % index at end of 1 cycle

time2_2=((t2_2-t1_2)/r)+time_2;                 % time at end of 1 cycle


%% DELIVERABLES

% Time
per = t2-t1;
per_time = per/fs;
rps = 1/per_time;
rpm = 60*rps;
deg=0:360/per:360;
deg=deg';

% Radius
R=zeros(t2,1);
for i=t1:t2
R(i) = 0.5*D_ref-0.5*x_ref +  ((z1(i,2)-V_ref)/K)+0.5*x_loc;
end

R(1:t1-1)=[];

rng = max(R)-min(R);
R_mid = min(R)+0.5*rng;
x_c = (max(R)-min(R))/2;
peak = deg(R==max(R));

display([z_loc, x_loc, x_c, R_mid, peak]')

rng2 = max(z1(t1:t2,2))-min(z1(t1:t2,2));
V_mid = min(z1(t1:t2,2))+0.5*rng2;

%Length%
per_2 = t2_2-t1_2;
per_time_2 = per_2/fs;
rps_2 = 1/per_time_2;
rpm_2 = 60*rps_2;
deg2=0:360/per_2:360;
deg2=deg2';

V_min=min(L1(:,2));
```

```
Lmax = (Z_peak-Z_ref)-((V_min-V_ref2)/K2);  %using backstop as reference Lref=0

L3=zeros(t2_2,1);
for i=t1_2:t2_2
   L3(i)=(Z_peak-Z_ref)-((L1(i,2)-V_ref2)/K2);
end
L3(1:t1_2-1)=[];


['z_loc =' num2str(z_loc), '  x_loc =' num2str(x_loc),'  x_c =' num2str(x_c),...
    '  R_mid =' num2str(R_mid),'  Peak =' num2str(peak), '  L_max =' num2str(Lmax)]

%% FIGURES
t3=(t2-t1)+t2;
t3_2=(t2_2-t1_2)+t2_2;

figure
plot(deg,z1(t1:t2,2),'b',deg,z1(t2:t3,2),'r') % next cycle overlaped (check)
title('next cycle overlap check')

figure
plot(deg2,L1(t1_2:t2_2,2),'b',deg2,L1(t2_2:t3_2,2),'r') % next cycle overlaped (check)

figure
plot(deg,R*25.4)
xlabel('Rotational Angle (Degrees)')
ylabel('Radius (mm)')
title(['Runout at Z = ' num2str(z_loc*25.4) 'mm ' 'and X = ' num2str(x_loc*25.4) 'mm'])
axis tight

figure
plot(deg2,L3*25.4)
xlabel('Rotational Angle (Degrees)')
ylabel('Length (mm)')
title('Length around the face of the part')

%%%%%%%%%%%%%%%%%%%%%%%%%%%%%%%%%%%%%%%%%%%%%%%%%%%%%%%%%%%%%%%%%%%%%%%

function [X,f]=spec(x,fs,whole)

% Computes the fft X of signal x and the corresponding frequency vector f given
% the sampling frequency fs.
% [X,f]=spec(x,fs)
% [X,f]=spec(x,fs,'whole') returns values around the whole unit circle

T=1/fs;
N=length(x);
X=T*fft(x);
f=[0:fs/N:(1-1/(2*N))*fs]';
if nargin == 2
 X=X(1:N/2+1,:);
 f=f(1:N/2+1,:);
end

%%%%%%%%%%%%%%%%%%%%%%%%%%%%%%%%%%%%%%%%%%%%%%%%%%%%%%%%%%%%%%%%%%%%%%%
```

```
function xp=zeropad(x,N);

% Pads an array with trailing zeros to length N
% xp=zeropad(x,N)

[m,n]=size(x);
if m > n
 xp=[x;zeros(N-length(x),1)];
else
 xp=[x,zeros(1,N-length(x))];
end
```

# APPENDIX C
# BENDING ANALYSIS

One consideration that was made, but not addressed in the above discussion, was the deflection of the tube during measurement due to flexure forces. Assuming the entire maximum expected force of 60 N is applied at the end of the hollow cantilever tube, and using the equation below, the maximum deflection is calculated to be 0.169 mm. Given the fact that the artifact was measured to within 0.041 mm, this amount of deflection seems extremely conservative. Nevertheless, it implies that an improvement to the design would be to substitute the aluminum tube for steel. This would produce a conservative deflection of 0.062 mm.

$$y_{max} = \frac{-Fl^3}{3\mathrm{EI}} \tag{C-1}$$

# LIST OF REFERENCES


[1] K. Brown, Personal interview. General Dynamics Ordnance and Tactical Systems. 18 Feb 2009.

[2] T. Yandayan, M. Burdekin, In-process dimensional measurement and control of workpiece accuracy, International Journal of Machine Tools and Manufacture 37 (1997) 1423.

[3] K. Vacharanukul, S. Mekid, In-process dimensional inspection sensors, Measurement 38 (2005) 204.

[4] T. Schmitz, K.S. Smith, Machining Dynamics Frequency Response to Improved Productivity. New York: Springer Science and Business Media, LCC 2009.

[5] G. Tlusty, Manufacturing Processes and Equipment. New Jersey: Springer Netherlands 1999.

[6] “efunda: Theory of Linear Variable Differential Transformer (LVDT).” http://www.efunda.com/designstandards/sensors/lvdt/lvdt_theory.cfm, accessed at University of Florida, 21 Feb 2010.

[7] “DCTH Series DC to DC LVDT Displacement Transducer.” http://www.rdpe.com/us/dcth.htm, accessed at University of Florida, 21 Feb 2010.

[8] S.T. Smith, Flexures Elements of Elastic Mechanisms. Florida: CRC Press, LLC 2000.

## BIOGRAPHICAL SKETCH

Arthur Graziano was born in São Paulo, Brazil to Renato and Thereza Graziano. He was raised in Orlando, FL and earned his Bachelor of Science degree in mechanical engineering at the Georgia Institute of Technology in May 2008. In July 2008 he joined the Machine Tool Research Center (MTRC) under the guidance of Dr. Tony Schmitz and received his Master of Science degree in May 2010.